Aalto University
School of Chemical
Engineering

Markus Luukkonen

Process modelling for the separation of light gaseous hydrocarbons produced by iron-catalysed Fischer-Tropsch synthesis

Master's Programme in Chemical, Biochemical and Materials Engineering
Major in Chemical Engineering

Master's thesis for the degree of Master of Science in Technology submitted for inspection,

Supervisor Professor Ville Alopaeus

Instructors D.Sc. (Tech) Kaj Jakobsson, M.Sc. (Tech) Miia Nevander

Aalto University
School of Chemical
Engineering

Author Markus Luukkonen

Title of thesis Process modelling for the separation of light gaseous hydrocarbons produced by iron-catalysed Fischer-Tropsch synthesis

Degree programme Master's Programme in Chemical, Biochemical and Materials Engineering

Major Chemical and Process Engineering

Thesis supervisor Professor Ville Alopaeus

Thesis advisor(s) D.Sc. (Tech) Kaj Jakobsson, M.Sc. (Tech) Miia Nevander

Date 25.09.2023 **Number of pages** 76 **Language** English

Abstract

Fischer-Tropsch synthesis produces a various number of off-gases, which require several separation processes to separate. This work focuses mostly on the separation of CO_2, as it is the most critical and complex.

The literature part focuses on comparing novel applications to more mature ones and it was found that deep eutectic solvents and hybrid membrane-absorption systems show a lot of promise towards commercializing. However, for the experimental part, already existing mature technologies had to be chosen, therefore amine absorption was picked, as it is widely used in flue gas applications.

The experimental part of the thesis covers all necessary separation processes and their operating conditions. A lot of experimenting in different operating conditions was done, and although amine absorption in literature tends to work better in higher pressures, as this raises the CO_2 partial pressure, in this work atmospheric pressure performed the best. The experimental part compares the performance of MEA (monoethanolamine), MDEA (methyldiethanolamine) and potassium carbonate.

When studying the results, MDEA was found to have the best capture efficiency with the equilibrium model, with MEA following close by.

Keywords Fischer-Tropsch synthesis, CO_2 separation, absorption

Tekijä Markus Luukkonen

Työn nimi Prosessimallinnus rautakatalysoidun Fischer-Tropsch synteesin tuottamien kaasujen erottamiseksi

Koulutusohjelma Master's Programme in Chemical, Biochemical and Materials Engineering

Pääaine Chemical and Process Engineering

Työn valvoja Professori Ville Alopaeus

Työn ohjaaja(t) TkT Kaj Jakobsson, TkM Miia Nevander

Päivämäärä 25.09.2023 **Sivumäärä** 76 **Kieli** englanti

Tiivistelmä

Fischer-Tropsch synteesi tuottaa monia eri poistokaasuja, joiden erotukseen vaaditaan useampia erotusvaiheita. Tämä työ keskittyy pääosin hiilidioksidin erotukseen, sillä se on vaikein ja kriittisin erotusvaihe.

Kirjallisuuskatsauksessa keskitytään vertailemaan uusia erotusmenetelmiä kypsiin menetelmiin. Kirjallisuuden perusteella voidaan todeta, että syväeutektiset liuokset ja yhdistelmä absorptiosta ja membraanierotuksesta ovat hyviä vaihtoehtoja, kun niiden kapasiteettia saadaan nostettua. Simulointiosiota varten tarvittiin jo olemassa oleva, kypsä vaihtoehto, joten amiiniabsorptio valikoitui, sillä sitä käytetään savukaasujen ja maakaasun puhdistuksessa.

Diplomityön simulointiosa kattaa kaikki erotusvaiheet ja niiden käyttöolosuhteet. Simulointeja ajettiin monissa eri olosuhteissa ja vaikka kirjallisuuden perusteella amiiniabsorptio toimii paremmin korkeammassa paineessa, kun hiilidioksidilla on korkeampi osapaine, työssä paremmin toimi ilmanpaine. Simulointiosiossa verrattiin MEA:n (monoetanoliamiini), MDEA:n (metyylidietanoliamiini) ja kaliumkarbonaatin erotustehokkuuksia.

Tuloksista käy ilmi, että MDEA:lla on paras erotustehokkuus tasapainomallilla simuloituna ja MEA:n tehokkuus seuraa lähellä perässä.

Avainsanat Fischer-Tropsch synteesi, CO_2-erotus, absorptio

Foreword

This master's thesis was carried out at VTT Technical Research Centre of Finland in the Future energy and process concepts team. The thesis was part of the ForestCUMP project and was completed between March and September of 2023.

I am grateful to have received the opportunity to work on such an interesting and important topic. I present my heartfelt thanks to my thesis supervisor, professor Ville Alopaeus, as well as my advisors D.Sc (Tech) Kaj Jakobsson from Aalto's side and M.Sc (Tech) Miia Nevander from VTT for their guidance, feedback and support. Additionally, I would like to thank Juha Lehtonen and Markus Hurskainen from VTT for providing advisor-like feedback and guidance during the thesis work. I also thank Juha-Pekka Pokki from Aalto for providing several great insights for the simulation part.

Finally, I extend my thanks to my family and friends for all their support and tolerance during my work on this thesis.

Table of contents

Used abbreviations

AEEA – Amino-ethylethanolamine
AMP – Amino-2-methyl-1-propanol
ASF – Anderson-Schulz-Flory
CCUS – Carbon capture, utilisation and storage
ChCl – Choline chloride
CPOX – Catalytic partial oxidation
DEA – Diethanolamine
DEPG – Dimethyl ether polyethylene glycol
DES – Deep eutectic solvent
DETA – Diethylenetetramine
EDA – Ethylenediamine
EOS – Equation of state
FT – Fischer-Tropsch
FTO – Fischer-Tropsch to olefins
FTS – Fischer-Tropsch synthesis
HBA – Hydrogen bond acceptor
HBD – Hydrogen bond donor
MDEA – Methyl diethanolamine
MEA – Monoethanolamine
MEA.CL – Monoethanolamine hydrochloride
MeOH - Methanol
MOF – Metal organic framework
MTO – Methanol to olefins
NMP – n-methyl-2-pyrrolidone
PC – Propylene carbonate
PSA – Pressure swing adsorption
PVDC – Polyvinylidene chloride
PZ – Piperazine
RWGS – Reverse water gas shift
SRK – Soave-Redlich-Kwong
TRL – Technology readiness level
VLE – Vapour-liquid equilibrium

1. Introduction

Environmental issues are a leading cause for process development in all sectors of industry, especially for the development of new sustainable processes. In 2020, the greenhouse gas emissions of Finland were 48.1 million tonnes of carbon dioxide equivalents (OSF, 2021). If the goal of reducing the amount by nearly 90% is to be met, which has been set for 2050, substantial changes must be done. These changes entail new innovations as well as upgrades on already existing technologies.

In 2018, the total plastic production was around 370 Mtons globally, of which only about 3.5 Mtons were bio-based. Furthermore, the market has only grown since and is expected to keep growing. (Bioplastics Magazine, 2020) Therefore, more sustainable plastic must be produced while also increasing the recycling rate. A statistic study (Statista, 2022) shows, that polyethylene and polypropylene make up a large amount of the plastic production. In 2021, the produced amounts of polyethylene and polypropylene were 107 Mtons and 75 Mtons, respectively. Both amounts are expected to grow by around 20 Mtons by the year 2029. (Statista, 2022) Coincidentally, nearly all of ethylene and propylene, which are the main materials for polyethylene and polypropylene, are produced by steam cracking. Steam cracking is an extremely endothermic process and causes around 300 Mtoe of CO_2 emissions per annum. (Amghizar et al., 2020, pp. 239-257)

One proposed method for sustainable polyolefin production is introduced in the ForestCUMP project, where CO_2 is extracted from flue gases. The CO_2 is fed into a reverse water gas shift (RWGS) reactor along with sustainably produced H_2 to produce syngas. Furthermore, the syngas is fed into a Fischer-Tropsch synthesis reactor, which in addition to the recycling of streams, results in olefins and paraffins, water, CO, CO_2 and H_2. This method would therefore be of great assistance for the goal of reducing CO_2 emissions, as flue gases would be utilised as a source of CO_2 for syngas. Furthermore, green hydrogen would be used, which makes the process environmentally friendly, ultimately resulting in green polyolefins. The general project concept is shown in Figure 1.

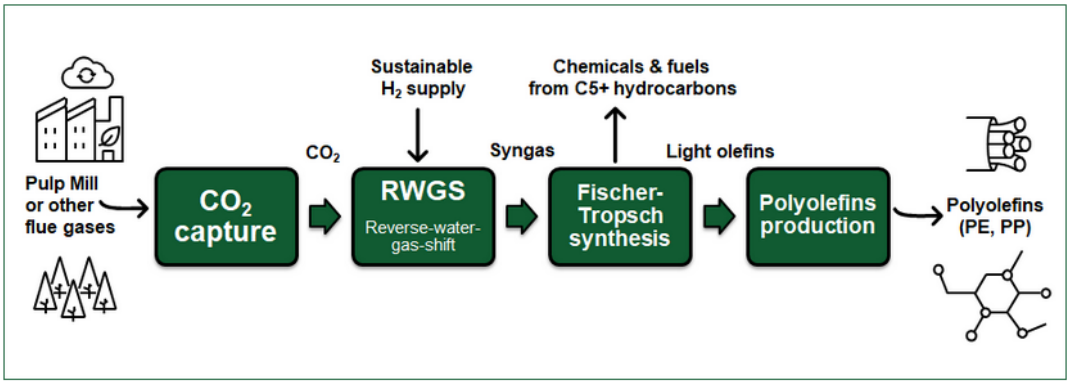

Figure 1. ForestCUMP project concept. (ForestCUMP, 2022)

The goal of the thesis is to find methods to separate light hydrocarbons from other light gases, ultimately resulting in olefins, paraffins, and C_{5+} hydrocarbons that could all be used in their own respective fields, while the light gases would be recycled back into the Fischer-Tropsch reactor. Light paraffin separation from olefins is not studied in this work, as they will be separated in an already existing distillation train further down the production line.

The focus of the literature part of this thesis is on the properties of the gases produced in the Fischer-Tropsch synthesis. Analysing the properties provides different possibilities for the separation of the gases, with the main focus being on the removal of CO_2. The methods will be reviewed in terms of maturity, technical parameters, and scalability into large-scale.

The experimental part will be done with the Aspen Plus simulator, with versions V11 and V12.1. The focus in the experimental part is going to be in the thermodynamics of the chosen separation processes, giving the mass and energy balances. Two of the methods that are found to be the most suitable during the literature review will be compared in the simulation part.

2. Properties of Fischer-Tropsch gases

Fischer-Tropsch synthesis (FTS) has been studied since 1923 and has become a catalytic process with large scale industrial applications. In the synthesis, syngas, consisting of CO and H_2, reacts on the surface of a catalyst, creating hydrocarbons and water. Hydrocarbons are formed following the Anderson-Schulz-Flory (ASF) distribution. (Rommens, and Saeys, 2023; Sohrabi et al., 2008) With iron-based catalysts, the selectivity towards lighter hydrocarbons can be tweaked by treatment and promoters. Furthermore, Fe catalysts are more suitable for FTS with high CO_2 content (Rommens, and Saeys, 2023), and they also promote selectivity towards light hydrocarbons, which is why an iron-based catalyst has been chosen for the project. The desired outcome is to separate light (C_2-C_4) hydrocarbons from the other light gases and C_5+ hydrocarbons. Light paraffins and olefins are not separated from each other, as they will be separated in an already existing distillation train further in the process. Figure 2 presents the mechanism in FTS (Saeys and Rommens, 2023) and Table 1 presents the melting and boiling points, and solubilities in water at 25 °C (PubChem, 2023) of all present main substances. Table 1 also shows the product composition, which are from simulations that used values from the studies by Feyzi et al. (2013) and Majone et al. (2010), after FTS. The simulation results from Table 1 have also included the recycling of streams as demonstrated later in Figure 3.

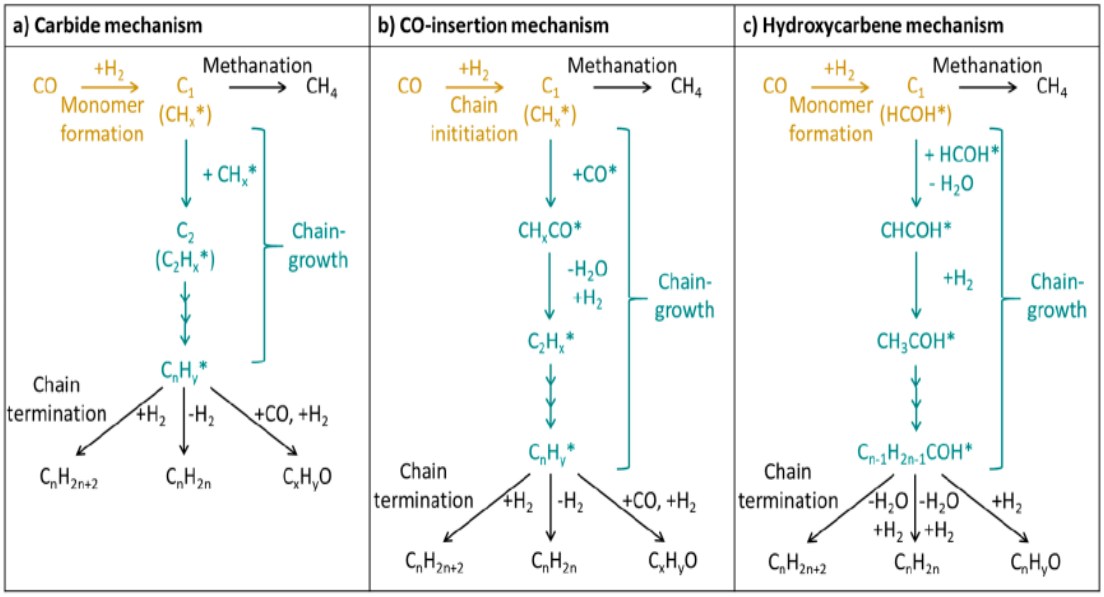

Figure 2. The three main mechanisms that take place inside an FTS reactor. (Saeys and Rommens, 2023)

Table 1. Melting and boiling points of all FTS off-gases in atmospheric pressure and gas composition.

Substance	Melting point (°C) (PubChem, 2023)	Boiling point (°C) (PubChem, 2023)	Solubility in water, mg/ml (PubChem, 2023)	w-% (Feyzi et al., 2013; Majone et al., 2010)
Water	0	100		21.4
Carbon monoxide, CO	-205	-191.5	Slightly soluble	19.42
Carbon dioxide, CO_2	Does not exist in atmospheric pressure.	-78.5	Slightly soluble	30.03
Hydrogen, H_2	-259.2	-252.8	Insoluble	2.57
Methane, CH_4	-182.6	-161.5	Insoluble	1.42
Ethane, C_2H_6	-182.8	-88.6	Insoluble	0.58
Propane, C_3H_8	-187.6	-42.1	Insoluble	1.13
n-Butane, C_4H_{10}	-138.3	-0.5	Insoluble	1.26
n-Pentane, C_5H_{12}	-129.7	36.1	Insoluble	0.02
n-Hexane, C_6H_{14}	-95.4	68.7	Insoluble	0.01
Ethene, C_2H_4	-169.2	-103.8	Insoluble	6.86
Propene, C_3H_6	-185.3	-47.7	Insoluble	2.83
1-Butene, C_4H_8	-185.3	-6.5	Insoluble	4.30
1-Pentene, C_5H_{10}	-165.2	29.9	Insoluble	1.08
1-Hexene, C_6H_{12}	-139.7	63.4	Insoluble	0.65
1-Heptene, C_7H_{14}	-119.7	93.6	Insoluble	0.85
1-Octene, C_8H_{16}	-101.7	121.2	Insoluble	0.1
Methanol	-97.8	64.7	1000, miscible	0.96
Ethanol	-114.1	78.2	1000, miscible	1.02
1-Propanol	-127	97.2	1000, miscible	0.93
1-Butanol	-88.6	117.6	68	0.69
1-Pentanol	-79	137.5	22	0.4
Acetic acid	-16.6	117.9	1000, miscible	0.74
Propanoic acid	-20.7	141.1	1000, miscible	0.51
Butanoic acid	-5.7	163.7	60, miscible	0.25

In Figure 2, in mechanisms a) and c), the monomer is also the chain-growth initiator, whereas in mechanism b) the initiation already begins in the addition of hydrogen on CO. As all the mechanisms state, C_nH_yO compounds are also created, indicating some amounts of carbonyls and alcohols, which are shown in Table 1. Different catalysts, such as Cu and Co alter the composition, as different metals are more selective towards other hydrocarbons.

Furthermore, from Table 1, it is easy to assume that all of the oxygenates and carbonyl compounds dissolve into water, thus making the separation easy. However, it is definitely worth taking a look at this issue, as some of the hydrocarbons are soluble in ethanol (PubChem, Ethene, 2023), and there is a substantial amount of ethanol present. This could make the separation complicated. The chosen process route is shown in Figure 3.

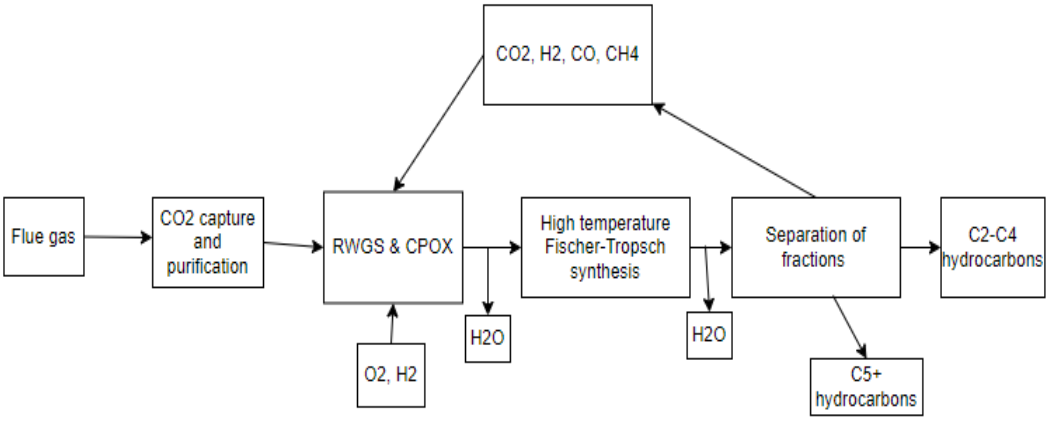

Figure 3. Chosen process route for this project.

As seen from Figure 3, CO_2 is captured from flue gases, then purified. The purified CO_2 is further fed into a RWGS reactor along with hydrogen and oxygen for catalytic partial oxidation (CPOX). From here, water is removed, and the acquired syngas is fed into a high-temperature Fischer-Tropsch synthesis. Now, from the existing fractions, C_5+ hydrocarbons, water, CO_2, H_2, CO and CH_4 must be separated. The result should be quite pure C_2-C_4 hydrocarbons, that can be further processed into polyolefins. The most problematic separation process is the removal of CO_2, as in terms of weight it is the dominating gas, while also easily forming dry ice. The phase diagram of carbon dioxide is shown in Figure 4.

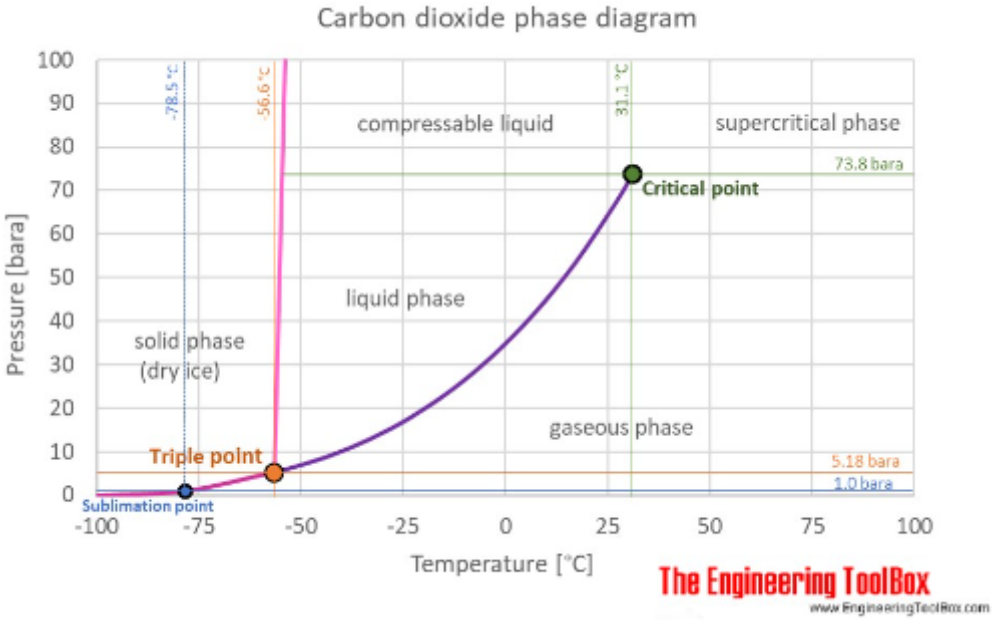

Figure 4. Carbon dioxide phase diagram. (ETB, 2018)

From Table 1 and Figure 4, it can be seen that distillation would not work as a separation process while CO_2 exists in the mixture. In the required temperature, CO_2 would form its solid dry ice phase, which would block the column. Furthermore, in higher pressures, CO_2 would form supercritical fluids with methane, making it a non-viable solution. However, several other options are available for review, such as absorption and adsorption technologies. It is of paramount importance to separate all unnecessary substances after FTS to produce clean polyolefins further in the process. The removal of CO_2 must happen after the synthesis, as the water-gas shift reaction that takes place inside FTS produces more CO_2.

Most of the problems in the separation of fractions lie in the separation of CO_2 as mentioned above. Additional problems could occur, if absorption is chosen for CO_2 separation and the removal of carbonyls and alcohols has been imperfect, as the mixture could form azeotropes further in the process. Furthermore, the gas has a unique composition in comparison to other applications, as its CO_2 content is over 30%, as demonstrated in Table 1. Table 2 compares the gas compositions of typical CO2 removal applications, such as flue gas and natural gas to the composition of the Fischer-Tropsch process assumed in this work.

Table 2. Comparison of gas compositions in typical CO_2 removal applications.

Substance/Application	Flue gas (natural gas-fired) (Song et al., 2004)	Flue gas (coal-fired) (Song et al., 2004)	Natural gas (Smithson, 2023)	Fischer-Tropsch (Feyzi et al., 2013; Majone et al., 2010)
CO_2	8-10%	12-14%	0-8%	30%
H_2O	18-20%	8-10%		21%
O_2	2-3%	3-5%	0-0.2%	
N_2	67-72%	72-77%	0-5%	
H_2				2.5%
CO				19%
Hydrocarbons			>80%	22%
Oxygenates				5.5%
H_2S			0-5%	
Argon, Helium			0-2%	

In Table 2, most of the natural gas hydrocarbons are methane, with the possibility of containing ethane, propane and butane, whereas in Fischer-Tropsch, they are mostly C_2-C_4 olefins and paraffins. However, as can be seen, the CO_2 content is clearly higher than in any other application. Due to these differences, it is possible, that those CO_2 removal applications that work for the other processes are not applicable for separation after Fischer-Tropsch.

3. Separation process options

In this chapter, separation process options will be reviewed. Subchapter 3.1 will be about separating gases other than CO_2, subchapters 3.2-3.7 are for CO_2 separation options and 3.8 will be a comparison subchapter, mainly for the CO_2 removal methods.

3.1 Separating of non CO2-gases

Recent studies, such as the ones from Zongbi et al. (2023) and Wu et al. (2023) show that the Fischer-Tropsch to olefins (FTO) and methanol to olefins (MTO) technologies have sparked additional interest in hydrocarbon separation methods. Although cryogenic distillation is the current “state-of-art” (Wu et al., 2023; Zongbi et al., 2023; Li et al., 2023). The open literature shows that there are new methods being researched. The most notable of these are metal organic frameworks (MOFs) (Wu et al., 2023; Zongbi et al., 2023), zeolites (Zongbi et al., 2023), porous carbon adsorbents (Zongbi et al., 2023), and heat-pump assisted distillation (Li et al., 2023).

The study of Li et al. (2023) claims that more research resources have been put into distillation due to its simpler construction and wider commercial use in comparison to other methods. Furthermore, the study presents a conventional process that is used in a Chinese refinery. In the system, they have 4 different columns. The first one runs with the highest pressure and lowest temperature, separating lighter components from the feed stream. The operating temperature increases and pressure decreases in each column, meaning that the second one runs on lower pressure and higher temperature, separating isopentane. The third column separates n-pentane, and the last one, having the lowest pressure and highest temperature, separates C_5+ hydrocarbons. The study used mixed integer non-linear programming and Aspen Plus to simulate and optimise heat-pump assisted distillation with dividing wall columns. The outcome of the study showed promise towards lower operating costs in a system, where multiple columns exist, but the technology is rather new. (Li et al., 2023)

The study of Zongbi et al. (2023) focused on extraction and separation of ethane and propane from natural gas with ultramicroporous carbon adsorbents. As their main

challenge they noted selectivity of separation, as it is difficult to fabricate uniform pores. They used polyvinylidene chloride (PVDC) resin derived ultramicroporous carbon as the experimental adsorbent. According to the study, carbon activated PVDC shows great potential in natural gas applications with high adsorption capacity, quick kinetics and robust stability. (Zongbi et al., 2023) Therefore, after further experiments on larger scale, these adsorbents could prove to be useful, if the selectivities of materials can be proven to be suitable. The study of Wu et al. (2023) supports the finding of higher adsorption capacity and faster kinetics in Zongbi's et al. (2023) study, while suggesting that the desorption kinetics is slow, resulting in higher energy losses during regeneration.

However, the study of May et al. (2012) suggests that in natural gas solutions just flashing is enough to separate C_2+ hydrocarbons and water from the system. Furthermore, the study by Kim and Do (2020) also states that after FTS, it is possible to condense and flash out C_5+ hydrocarbons and water. Technically, water would be condensed in a condenser, after which the system would be cooled down even more to separate C_5+ hydrocarbons from the mixture, which is shown by Kim and Do (2020) to also work in simulations in a large, industrial scale.

The HISORP system of Linde Engineering (Linde Engineering c, n.d.) also appears promising for hydrocarbon recovery, as they use temperature swing adsorption (TSA) with at least 3 adsorber units to recover C_5+ hydrocarbons and water. Essentially, the gas flows from the top to the bottom and adsorbs on the adsorbent. Once fully loaded, the adsorber undergoes heating and cooling in order to regenerate and heavier hydrocarbons and water will be separated with a condensate separator. Regeneration gas is recycled, as it contains valuable components that should not go to waste. Furthermore, they also have a similar system for hydrogen separation. (Linde Engineering a; c, n.d.)

Optimally, methane would be separated from the other light gases that can be fed back to the CPOX reactor, even though methane can also be returned. However, this would likely require a larger reactor and therefore raise the capital expenditures. Therefore, some of the methane could be burned and the generated heat could be used in amine regeneration or other energy intensive steps. In the case of burning methane, as little as possible pure hydrogen should be present, as it is a valuable

resource. The remaining methane can be reformed back to syngas (Maitlis and de Klerk, 2013).

The book by Maitlis and de Klerk (2013) suggests that Fischer-Tropsch tail gas is usually fed into a cryogenic separator once water and CO_2 are out of the system, as they would form solid phases during cryogenic separation. The column would separate the hydrocarbons from methane, hydrogen, and CO. An open loop plant design is beneficial in cryogenic C_2+ separation, as tail gas recycling could be expensive. (Maitlis and de Klerk, 2013) The study of Kim and Do (2020) further supports the use of a cryogenic separator, as they studied a flash tank at -90 °C and 40 bar, after which followed a further purification step of a distillation column at -114 °C in order to achieve a high purification level for the hydrocarbons. According to the results of the study, this was successful.

3.2 Separation of CO_2, amine applications

Amine absorption is highly corrosive, as the degradation of amines leads to compounds that can destroy the system within days (Baker & Lokhandwala, 2008). With amine absorption, the removal of CO_2 happens in a two-step mechanism. Firstly, gas dissolves into the aqueous amine solution followed by the reaction of the weak base (amine) and weak acid (CO_2) into carbamate. The partial pressure of CO_2 in gas feed controls the reaction. (May et al., 2012) The reactions taking place are presented in Equations 1-5, that are valid for MEA absorption. The equations consist of water dissociation reaction and reactions between monoethanolamine (MEA), water, and CO_2. (Chen et al., 2011)

$$2H_2O \rightleftharpoons H_3O^+ + OH^- \quad (1)$$

$$MEAH^+ + H_2O \rightleftharpoons MEA + H_3O^+ \quad (2)$$

$$MEACOO^- \rightleftharpoons MEA + HCO_3^- \quad (3)$$

$$CO_2 + 2H_2O \rightleftharpoons H_3O^+ + HCO_3^- \quad (4)$$

$$HCO_3^- + H_2O \rightleftharpoons H_3O^+ + +CO_3^{-2} \quad (5)$$

The reactions show that the pH of the amine solution controls the reactions and therefore the pH is an important parameter to control. The carbamate formation reaction is the dominating reaction for primary and secondary amines (May et al.,

2012) such as MEA and diethanolamine (DEA), which are two of the most commonly used amines for CO_2 separation (Alnashef et al., 2017). According to the study by May et al. (2012), the capacity to absorb CO_2 for primary and secondary amines is around 0.5 mol CO_2 per mole of amine. Another study by Kidnay and Parrish (2006) suggests that DEA-based processes could reach higher loading through the partial hydrolysis of carbamate to bicarbonate, regenerating some amine, shown in Equation 6.

$$RNHCOO^- + H_2O \rightleftharpoons HCO_3^- + RNH_2 \quad (6)$$

Tertiary amines lack the hydrogen bonded to the central nitrogen atom and therefore cannot directly form carbamate by reacting with CO_2. Therefore, the reaction of Equations (2) and (3) must take place, giving the overall reaction shown in Equation 7. (May et al., 2012)

$$RR'R''N + CO_2 + H_2O \rightleftharpoons RR'R''NH^+ + HCO_3^- \quad (7)$$

Where R is the primary carbon chain, R' is the secondary carbon chain and R'' is the tertiary carbon chain.

The study by May et al. (2012) suggests that tertiary amines could achieve a higher load of CO_2 per mole of amine than primary and secondary amines, while also requiring less heat to regenerate. Furthermore, the reaction kinetics are slower for tertiary amines. Process flow diagram of a methyl diethanolamine based process shown in Figure 5, which is also applicable for other amines and hot carbonate. (May et al., 2012)

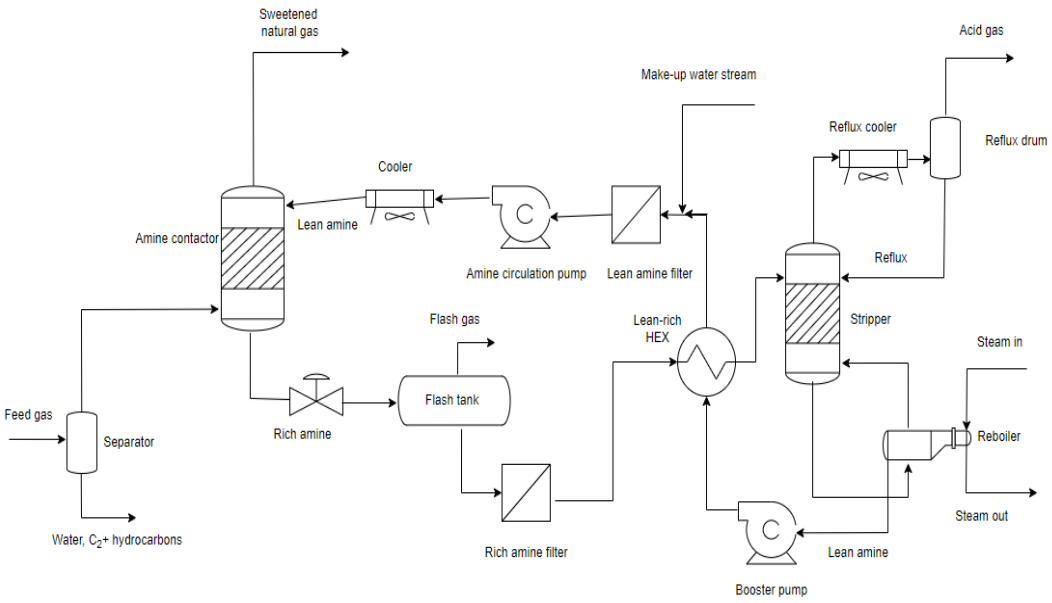

Figure 5. Process flow diagram of a typical amine solvent based chemical adsorption system for the separation of CO_2 and other acid gases from natural gas. Reproduced from May et al. (2012) Fig. 2.

It is worth noting that Figure 5 represents the removal of CO_2 from natural gas, meaning that in the first separator, most C_2+ hydrocarbons are separated from the feed, whereas post FTS, the desired final product is exactly C_2-C_4 hydrocarbons, meaning that only C_5+ hydrocarbons should be separated. However, the same process principle could still be applied.

Lee et al. (2016) studied the effects of amine blends on the activation and reaction energies of CO_2 absorption. The amines they used were MEA, DEA, 2-amino-ethylethanolamine (AEEA), amino-2-methyl-1-propanol (AMP), diethylenetetramine (DETA), and piperazine (PZ). The most notable findings were that CO2 absorption was increased with blended solvents through the lowered activation energy caused by the extra molecules of amine/water. The extra molecules were claimed to strengthen the intermolecular interactions, which enhances withdrawing of the proton from the amine. Furthermore, PZ, AEEA, and DETA were reported to enhance the performance of MEA, while AMP and DEA hinder the CO_2 absorption capabilities. (Lee et al., 2016) Therefore, perhaps the capabilities of different amine blends could be interesting to study in the experimental part.

3.3 Hot carbonate

Hot carbonate process shares most of the features with the amine process that was presented in Figure 5 (May et al., 2012; Speight, 2007). The process has been successfully used for separating CO_2 from various gas mixtures such as ammonia, natural gas and ethylene oxide plants for decades (Smith et al., 2016; Speight, 2019). Smith et al. (2016) studied the Benfield process, which was created by Benson and Field in the 1950s. Furthermore, the Benfield is in full use in a Chinese factory, as shown in the study of Maitlis and de Klerk (2013). In the study of Smith et al., (2016) it was believed that there would be no need for temperature swing, as CO_2 would regenerate solely from the pressure swing between absorption and desorption. (Smith et al., 2016)

Speight (2007) revisited his earlier studies from 1993 and researched carbonate washing. He found out that the absorption rate of CO_2 in potassium carbonate, K_2CO_3, increases with temperature. The reaction between potassium carbonate, carbon dioxide, and water is shown in Equation 8. (Speight, 2007)

$$K_2CO_3 + CO_2 + H_2O \rightleftharpoons 2\,KHCO_3 \tag{8}$$

In the light of Speight's (2007) study, the absorption process functions at its best near the reversibility temperature of around 120 degrees Celsius, while regeneration is activated by lowering the pressure and/or raising the temperature. As a drawback, Speight mentions that potassium carbonate also absorbs hydrocarbons in relatively high quantities. However, in natural gas solutions it can decrease the acid gas content, which can be assumed to be CO_2 in this case, from 50% to as low as 0.5%. (Speight, 2007) According to Kohl and Nielsen (1997), MEA or DEA could be used to improve the absorption rate of CO_2 in potassium carbonate, while also increasing mass transfer rates. (Kohl & Nielsen, 1997)

3.4 Deep eutectic solvents

According to a study by Choi et al. (2016), deep eutectic solvents (DESs) tend to work best, when a hydrogen bond acceptor and donor (HBA, HBD) are present. In the study, more acidic DESs showed more promise towards CO_2 selectivity. Furthermore,

the highest CO_2 solubility was achieved by using ethylenediamine [EDA] as HBD and monoethanolamide hydrochloride [MEA.CL] as HBA. Additionally, higher ratios of [EDA]:[MEA.CL] showed better solubility of CO_2, and the ratio of 3:1 was deemed to be the best fit. In 2.5 minutes, a solution with the forementioned ratio was able to absorb 25.2 w-% CO_2. In the study it was also pointed out that pure [EDA] turns gel-like quite easily, resulting in loss of CO_2 uptake after approximately 30 minutes. Pure amines in large-scale processes also tend to exhibit corrosive behaviour, which supports choosing DESs over pure amines. The absorption mechanism of [MEA.CL]:[EDA] is based on the hydrogen bonding between [EDA] and CO_2, forming carbamate. (Choi et al., 2016) However, the study was done for CO_2 capture from flue gases, so it remains unsure how suitable it is for post FTS CO_2 capture. The suitability for large scale absorption also remains unknown.

The study of Jahanbakhsh-Bonab et al. (2022) shows promise towards methyl diethanolamine (MDEA) DESs as a replacement for conventional amine absorption in natural gas sweetening. Natural gas can be treated as a similar mixture to FT product gas. They show increased solubility and diffusivity selectivities than aqueous MDEA. In the study, the solubility seemed to increase as a function of pressure. (Jahanbakhsh-Bonab et al., 2022) Another study by Alnashef et al. (2017) researched DESs with amines and choline chloride (ChCl) as the HBD. The study showed that ChCl-MEA was the most promising combination for dissolving CO_2. Figure 6 presents the effect of ChCl : MEA molar ratio on the solubility of CO_2. (Alnashef et al., 2017)

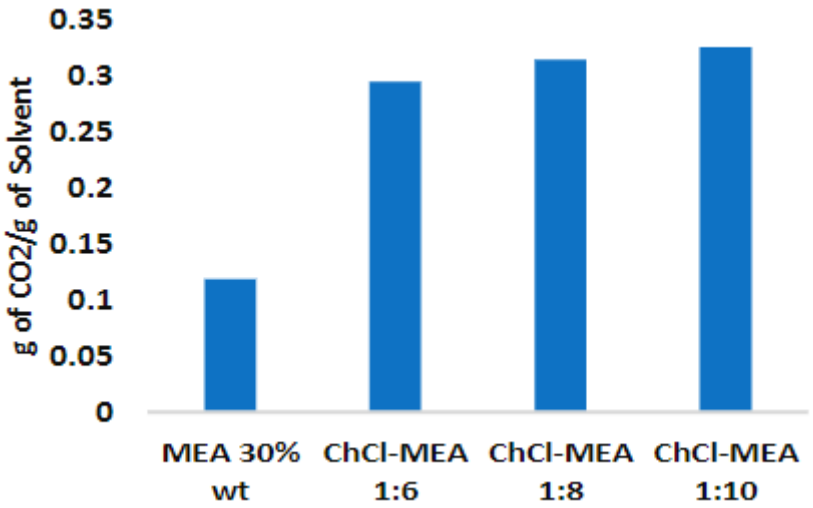

Figure 6. Effect of molar ratio on the solubility of CO_2 in ChCl-MEA. (Alnashef et al., 2017, Fig. 6, p. 1399)

The study of Alnashef et al. (2017) and Figure 6 further support the findings of better CO_2 solubility with DESs in the study by Choi et al. (2016). Moreover, Alnashef et al. (2017) also conducted their study on combustion gases, so in this case it also remains unsure if the method is usable post FTS, as DESs could also dissolve the desired end products.

3.5 Physical solvents

May et al. (2012) also mentioned the use of physical solvents, such as dimethyl ether polyethylene glycol (DEPG, Selexol™), n-methyl-2-pyrrolidone (NMP, Purisol®), methanol (MeOH, Rectisol®) and propylene carbonate (PC, Fluor solvent™) for CO_2 removal from natural gas. Table 3 represents the relative solubilities of various components in these solvents (Burr and Lyddon, 2008).

Table 3. Relative solubilities of various components in physical solvents. Reproduced from Burr and Lyddon (2008).

Component	PC, 25 °C	DEPG, 25 °C	NMP, 25 °C	MeOH, -25 °C
CO_2	1.0	1.0	1.0	1.0
H_2	0.0078	0.013	0.0064	0.0054
CO	0.021	0.028	0.021	0.020
Methane	0.038	0.066	0.072	0.051
Ethane	0.17	0.42	0.38	0.42
Ethene	0.35	0.47	0.55	0.46
Propane	0.51	1.01	1.07	2.35
i-Butane	1.13	1.84	2.21	-
n-Butane	1.75	2.37	3.48	-

As can be seen from Table 3, the relative solubilities of C_3+ hydrocarbons are higher than CO_2. In natural gas this does not matter, as the desired outcome consists mostly of methane. However, the desired products of this work are C_2-C_4 hydrocarbons and therefore these physical solvents cannot be used, as major amounts of the desired products would dissolve into the solvents, making it economically unsustainable, while also requiring an additional separation step.

3.6 Membrane filtration

In their study, Mittal et al. (2015) state that the problem of membrane separation is lower efficiency than in amine separation. This is due to contaminants, concentration polarisation, permeability/selectivity trade-off, aging, and plasticisation. Thus, pretreatment before membrane separation is of paramount importance. The most problematic contaminants are water and heavy hydrocarbons. Water causes membrane swelling, which compromises the whole integrity of the membrane. Furthermore, heavy hydrocarbons can form a film around the surface of the membrane, decreasing the permeation rate substantially. (Mittal et al., 2015)

Mittal et al. (2015) propose that the biggest obstacle that polymeric membranes face, is the trade-off of permeability and selectivity. This is due to the inverse proportionality of permeability as a function of selectivity, which was studied by Robeson (1991). A

study by Koros et al. (1988) suggests that decreasing gas permeability would increase selectivity. However, another study by Scholes et al. (2017) suggests that thermal rearrangement of polymeric membranes could increase CO_2 selectivity without altering their permeability.

According to a study by Paul et al. (2014), thick and thermally reduced polymers inhibit significant decline of permeability. However, when exposed to ethane, ethene and propane, ageing of the thick membrane accelerated and polymer matrix started plasticising. (Paul et al., 2014) Glassy membranes are better for CO_2 selectivity (Mittal et al., 2015; Baker and Lokhandwala, 2008), therefore plasticisation should be avoided, as it will increase selectivity towards C_3+ hydrocarbons (Baker & Lokhandwala, 2008; Hoorfar and Alcheikhhamdon, 2017).

Initially, anisotropic cellulose acetate membranes were used for separation. In the late 1990s, polyimide and perfluoropolymer membranes rose to compete. In anisotropic membranes, the same polymer is used for the selective layer and the microporous support layer. However, for composite membranes the microporous support layer is coated by a different material to create the selective surface layer. Currently, either flat-sheet packaged spiral-wound or hollow fiber modules are being used for CO_2 separation. Hollow fiber modules are more capable of fitting a larger membrane area in a smaller package. However, spiral-wound modules tend to exhibit higher permeance, compensating for the higher cost per area. (Baker and Lokhandwala, 2008)

A study by Hoorfar and Alcheikhhamdon (2017) compares cellulose acetate, polyimide, and fluoropolymer membranes. According to them, fluoropolymer membranes require the least pretreatment, while polyimide membranes require the most pretreatment. Furthermore, the most widely used fluoropolymer membranes for CO_2 extraction are Teflon-based. Some parameters of the membranes are shown in Table 4. (Hoorfar and Alcheikhhamdon, 2017)

Table 4. Studied membrane parameters. Reproduced from Hoorfar & Alcheikhhamdon (2017).

	Cellulose acetate	Polyimide	Fluoropolymer
Commercialised	Mid 1980s	1994	2008
Commercial name	Separex®/CYNARA	MEDAL	Z-Top
Module	Spiral wound/Hollow fiber	Hollow fiber	Spiral wound
Barrer CO_2 permeability	6	11.5	150+
Studied CO2/CH4 selectivity	12-15 (moderate)	20-25 (high)	6.5 (low)
Solid fouling resistance	Moderate	Depends on manufacturing	High
Plasticisation resistance	Moderate	Depends on manufacturing	High
Water resistance	Low	Depends on manufacturing	High
Pre-treatment required	Standard	Extensive	Low
Research potential	Low, mature technology	Moderate in performance sustainability	Moderate in performance enhancement

From Table 4 it can be observed that the trade-off of permeability and selectivity mentioned by Mittal et al. (2015) somewhat applies here too, with polyimides defying the inverse proportionality, having a higher permeability and selectivity compared to cellulose acetate membranes. In the light of the study of Hoorfar and Alcheikhhamdon (2017) and Table 4, it seems that any of these could be used, as they are used for natural gas sweetening.

In the light of this work, Linde Engineering (Linde Engineering a, n.d.) has developed an attractive technology for membrane separation as well as separating water and C_5+ hydrocarbons from the mixture (Linde Engineering c, n.d.). The suggested technology utilises hollow fibers for a tight packing, while also only being a single-

stage process and offering a high selectivity. Furthermore, Linde's HISELECT technology tolerates high CO_2 partial pressures and has a long membrane lifetime (Linde Engineering b, n.d.), making it a great alternative for CO_2 separation and purity of retentate gas. Estimated plant lifetime in comparison to a standard cellulose acetate membrane is shown in Figure 7, while flow inside the membrane is shown in Figure 8.

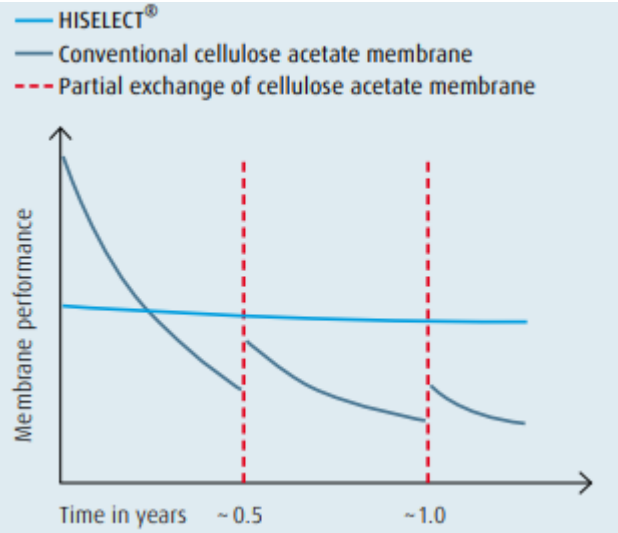

Figure 7. HISELECT membrane lifetime in comparison to a conventional cellulose acetate membrane. (Linde Engineering b, n.d.)

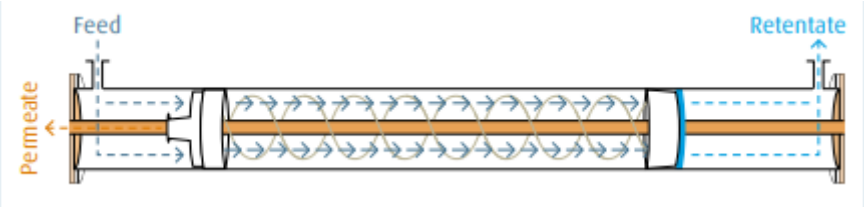

Figure 8. General flow inside the membrane. (Linde Engineering b, n.d.)

As seen from Figure 7, with the HISELECT technology, the membrane performance stays on a similar level for much longer, eliminating the need for constant replacement that happens with cellulose acetate membranes. Even though conventional methods seem to exhibit better initial performance, HISELECT seems to outperform them in the long run.

3.7 Hybrid membrane-absorption system

A study (Rezakazemi et al., 2017) was conducted on a hybrid membrane-absorption system for natural gas sweetening. In the system, amine absorption would follow the membrane, where most of the CO_2 would be removed. According to the study, solely amine absorption is suitable for feeds with 5-11% CO_2, while the hybrid system would be suitable for feeds with >11% CO_2. Moreover, the study suggests that membranes are suitable, when the flow is between 6 000 and 30 000 m^3/h. (Rezakazemi et al., 2017)

Another study by Kim and Do (2020) also suggests that a membrane filtration followed by amine absorption could be beneficial in terms of operating costs and effectiveness. In the study, CO_2 separation could be achieved by sequentially integrating membrane and absorption technologies. Commercially, amine-based absorption is used for the removal of CO_2, but it is not a perfect solution. Furthermore, operating costs of amine-based absorption are relatively high, due to the high energy consumption rate of amine regeneration. However, it was mentioned that absorption could be accompanied by a hollow fiber cellulose acetate membrane. This has substantially lower production costs and it removes and recovers the majority of CO_2 and H_2. After the membrane, absorption can be used to further reduce the CO_2 content to the required level. After this step follows cryogenic de-methanisation, where the light hydrocarbons are liquefied and collected for further downstream use. This resulted in C_2-C_4 production costs of 3.58 $/kg, and -1.85 kg of CO_2 per 1 kg of produced C_2-C_4, meaning that one kilogram of light hydrocarbons would simultaneously dispose of 1.85 kilograms of CO_2. The price of green H_2 is considered as the most sensitive and dominant factor in the costs. (Kim and Do, 2020)

3.8 Adsorption

In the study by May et al. (2012), adsorption was mentioned as one of the up-and-coming methods for CO_2 removal. The adsorbents mentioned in the study included activated carbons, zeolites, zeolitic frameworks and metal organic frameworks (MOFs) as the most potent competitors in terms of capacity, while activated carbons and MOFs exhibited the highest CO_2/CH_4 selectivities. However, MOF use in industrial scale was unsure due to its availability and poor stability chemically and

thermally. (May et al., 2012) Furthermore, these adsorbents were only studied with feeds under 12 000 m^3/h, therefore their suitability for higher feeds remains unsure.

A more recent study on MOFs by Telfer et al. (2021) shows that the CO_2/CH_4 selectivity with a new MUF-16 MOF has risen to 6690, while the CO_2/C_2H_2 selectivity was 510, suggesting that the losses of light hydrocarbons would be minimal. These selectivities far exceed those of MOFs with open metal sites (Telfer et al., 2021, Supplementary Tables 10 and 11). However, the study still suggests that the scalability and separation capabilities of MUF-16 leave a lot to be desired even though the technology has advanced greatly from 2012. Furthermore, the study was conducted only in laboratory scale, and it remains unknown if it would be possible to scale up even though the materials to construct MUF-16 are economical even in large scale production. Structures of MUF-16 MOFs presented in Figure 9. (Telfer et al., 2021)

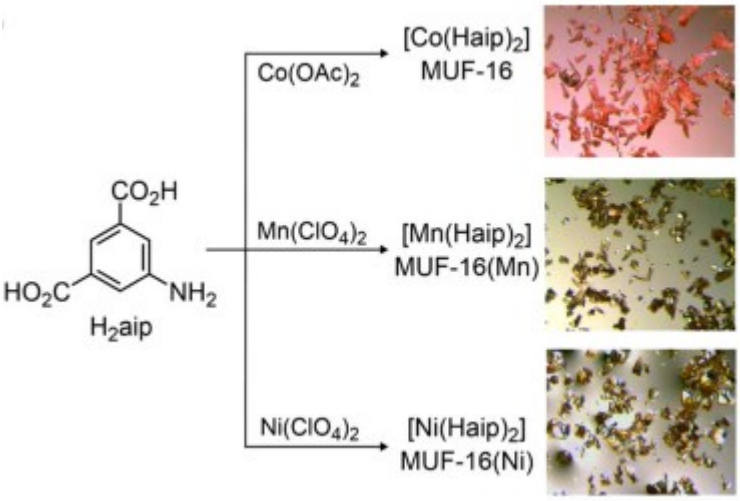

Figure 9. The structure and micrographs of different MUF-16 MOFs. (Telfer et al., 2021)

The MOFs in Figure 9 are porous, and the pores are deliberately constructed to match CO_2 molecule size and electrostatic potential. This allows for the pores to trap CO_2 molecules efficiently by noncovalent interactions and hydrogen bonding. (Telfer et al., 2021) Furthermore, in a study by Chakraborty and Kayal (2018) they found that a chromium-based MOF with some (1 m-%) activated carbon works best in low temperatures and high pressures. Nevertheless, based on the forementioned

aspects, the method could end up being promising in the future, but not worth further investigating as of now.

The studies of Bastos-Neto et al. (2017) and Grande et al. (2017) researched the possibility of pressure swing adsorption (PSA) for CO_2 removal. Bastos-Neto et al. (2017) studied capturing CO_2 from flue gases with an activated carbon adsorbent and came to the conclusion that it is feasible when the CO_2 volume fraction is more than 0.05 and less than 0.15. Simulation results and experimental data were quite close to each other. (Bastos-Neto et al., 2017) On the other hand, the study of Grande et al. (2017) was focused on natural gas with a feed of 500 000 Nm^3/h and a composition of 10% CO_2. They tried out a 12 column PSA system with CO_2 recovery reaching nearly 85% with a carbon molecular sieve. Furthermore, they mentioned that with a higher partial pressure (higher CO_2 loading), higher recovery might be possible, but there is no certainty. (Grande et al., 2017)

3.9 Comparison of separation processes

This chapter will be mainly about comparison of the CO_2 removal processes as much as it is possible to compare them and summarising their pros and cons. Comparison of maturity, scalability, further research possibilities, and commonly used applications are shown in Table 5.

Table 5. Comparison of maturity, scalability and further research possibilities of the different CO_2 removal methods.

Method	Maturity	Scalability	Further research possibilities	Commonly used applications (Kearns et al., 2021)
Amines	Widely used for all kinds of CCUS applications, technology readiness level (TRL) 9 (Hong, 2022; Tcvetkov, 2021)	Usable in small and large scale and various compositions of gases. (May et al., 2012)	Not much, perhaps amine blends for better environmental friendliness	Fertiliser, soda ash, natural gas processing plants
Hot carbonate (Benfield process)	Also in wide commercial use, quite the same mechanism as with amines; TRL 9 (Kearns et al., 2021)	The same as amines applies here.	Not much, also perhaps researching blends with other substances to enhance absorption.	Fertiliser plants, natural gas solutions (UOP, n.d.)
DESs	Falls into the category of ionic liquids, only at lab testing scale, TRL 2-3 (Kearns et al., 2021)	Unknown, as only lab tests have been conducted.	A lot, studies (Jahanbakhsh-Bonab et al., 2022; Alnashef et al., 2017) show higher absorption capabilities than amines, while being more environmentally friendly. Also, a high number of ionic liquids exist.	Lab testing
Membranes	Separation membranes for natural gas; TRL 9. Polymeric membranes; TRL 7. (Kearns et al., 2021)	Able to use in all kinds of scales, can use different kinds of packing (Hoorfar and Alcheikhhamdon, 2017)	There are possibilities of researching hybrid systems with membranes, as Air Liquide and Linde Engineering are	Natural gas processing, pilot studies

			doing (Kearns et al., 2021)	
Hybrid systems	Ranging from TRL 2-6. Polymer membranes + cryogenic separation at 6, solvent hybrid at 4. (Kearns et al., 2021)	Unknown, pilot studies are being conducted, but polymer membrane + solvent hybrid seemed to work in large scale in simulations (Kim and Do, 2020)	Same as above.	Conceptual studies, pilot studies
Adsorption	Zeolitic PSA TRL 9 in flue gas solutions (Kearns et al., 2021; Tcvetkov, 2021) MOFs TRL not available, not stable enough (Wang et al., 2023)	PSA is available in large scale (Riboldi and Bolland, 2017); MOFs in lab testing	Better adsorbents can be found. In the case of MOFs, the possibility is in finding a way to make them stable enough to be able to duplicate them.	Large pilot tests and flue gas applications
Physical solvents (Selexol, Rectisol)	TRL 9 in natural gas solutions and coal gasification plants (Kearns et al., 2021)	Available in small and large scales (May et al., 2012)	Not much left to research apart from new solvents with different selectivities.	Natural gas processing, coal gasification plants

Table 5 shows that the most mature technologies are amines, hot carbonate, membranes, adsorption and physical solvents. Scalabilities of all mature methods are found to be similar.

Physical solvent technologies, such as Rectisol and Selexol have successfully been used in natural gas applications in large-scale for a long time (May et al., 2012) and the TRL value also suggests this with a value of 9 (Kearns et al., 2021). They could be more environmentally friendly compared to amines, but the drawback is the fact that they dissolve more propene and butene than CO_2 (Burr and Lyddon, 2008), making it unviable for post FTO CO_2-removal.

Deep eutectic solvents showed a lot of promise towards better CO_2 absorption capabilities in the studies of Choi et al. (2016), Jahanbakhsh-Bonab et al. (2017) and Alnashef et al. (2017). However, as these are limited to lab-scale testing (Kearns et al., 2021), they are not going to be modelled in this work.

In adsorption, the adsorbents used in PSA are quite simple and economical compared to amines that are highly toxic, as adsorbents are mostly either zeolites or activated carbon. However, the TRL of PSA is related to flue gases and not natural gas or FTO process. Furthermore, it could potentially be unsuitable for such a large-scale process with a CO_2 content of over 30 w-% (Grande et al., 2017; Bastos-Neto et al., 2017). Furthermore, the study of Bastos-Neto et al. (2017) showed that nearly 15 v-% of the CO_2 stays in the product stream with the desired products, even when the feed only contains 10 v-% CO_2. Additionally, Grande et al. (2017) mention that PSA is 40% more costly than amines although a study by Riboldi and Bolland (2017) conflicts with this, showing the same electric efficiency for MEA based absorption and PSA with zeolites.

A hybrid system has been modelled by Kim and Do (2020) and their study showed great promise towards an economical and ecological system. However, being only at TRL 4 (Kearns et al., 2021), a hybrid system is not going to be modelled in this work, but is worth keeping in mind for the future, as further research by Linde Engineering and Air Liquide in the HISORP and HISELECT technologies could prove to show improved scalability (Linde Engineering, a, b, c, n.d.).

Metal organic frameworks would be a great adsorption technology if they were stable and easily duplicatable. They show great selectivity towards CO_2 and are able to adsorb high loads, when pretreated correctly. (Telfer et al., 2021) Thus, this is also a method that should be kept in mind for the future, as selectivity is an important factor in FTO applications to make them viable.

Membranes are found to be a satisfying alternative, but as the required degree of CO_2 removal is at least 99%, it is unlikely that membranes alone could achieve this level (Mittal et al., 2015; Kim and Do, 2020). However, the Linde Engineering HISELECT process (Linde Engineering c, n.d.) sounds promising, as they mentioned 99%

removal, but without any further knowledge on the parameters and suitability for post FTO process, it is impossible to model in Aspen.

The differences of hot carbonate and amine processes could be interesting to analyse in simulations, as they follow the same principle. Furthermore, the differences of amines and amine blends for CO_2 absorption could be interesting to investigate, as a base has already been offered by Lee et al. (2016).

4. Thermodynamic methods

The Aspen Plus simulator has access to a vast number of databanks (NIST, DIPPR) and conducted vapour-liquid equilibrium (VLE) data studies of components. Therefore, strong regression models can be made to estimate the behaviour of the ternary system based on the databanks (Nakagaki et al., 2019). However, some parameters could be outdated or have the wrong input, and therefore it is important to check recent, or benchmark studies and compare those parameters with those in Aspen. Great comparison points are offered in the studies of Nakagaki et al. (2019) and Chen et al. (2011), with those studies having solved an extraordinary number of parameters and other important data.

As the CO_2 separation process involves water dissociation when using absorption and has ionic interactions, it is an electrolyte system, as pointed out earlier in Equations 1-5. Therefore, a thermodynamic model that calculates electrolyte systems must be chosen. For this, the e-NRTL model is a strong candidate, as it can fit parameters into experimental data within known temperature and concentration ranges, which have been extended in the study of Nakagaki et al. (2019). Additionally, CO_2 has a relatively high partial pressure in the process and therefore an equation of state (EOS) model must be used for the gas phase. The Soave-Redlich-Kwong EOS is widely used for hydrocarbons in elevated pressures as it is a quite simple, but accurate model (Skogestad et al., 2016). However, this relies on the fact that binary interaction parameters are available. Therefore, choosing the eNRTL-RK model is logical, as the package has both, the eNRTL model and the SRK EOS. These should also be fitting for the separation of heavier hydrocarbons and water, and other light gases as well, although a comparison with UNIFAC could be worthwhile for the separation of heavier hydrocarbons and water, as it predicts liquid-liquid equilibrium a bit better in a polar system with alcohols.

As specific heat capacity and VLE parameters are both dependant on the equilibrium composition, they are regressed together in the study of Nakagaki et al. (2019). Equations for equilibrium constant and Gibbs free energy change are presented in Equations 9 and 10.

$$K = \prod_i (a_i)^{v_i} = \prod_i (x_i \gamma_i)^{v_i} \quad (9)$$

$$-RT\ln K = \Delta_r G = \Delta_r H - T\Delta_r S \quad (10)$$

where K is the equilibrium constant of a reaction, a_i is the activity of component i, v_i is the stoichiometric coefficient of component i, x_i is the mole fraction of component i, γ_i is the activity coefficient of component i, R is the universal gas constant, T is the system temperature, $\Delta_r G$ is the change in Gibbs free energy, $\Delta_r H$ is the standard enthalpy of reaction, and $\Delta_r S$ is the change in entropy. The eNRTL model calculates ion-ion interactions, which can be presented as Pitzer-Debye-Hückel and Born equations, shown in Equations 11-13.

$$\frac{G_m^{ex}}{nRT} = \sum_{j=m,c,a} X_j \left(\frac{\sum_{i(\neq j=c,a)} X_i \tau_{ij} G_{ij}}{\sum_{i(\neq j=c,a)} X_i G_{ij}} \right) \quad (11)$$

$$G_{ij} = e^{-\alpha_{ij}\tau_{ij}} \quad (12)$$

$$\tau_{ij} = a_{ij} + \frac{b_{ij}}{T} + e_{ij}\ln T + f_{ij}T, \tau_{ii} = 0 \quad (13)$$

where G_m^{ex} is the excess Gibbs energy, τ_{ij} is the asymmetric binary interaction energy parameter, α_{ij} is the symmetric non-randomness factor that can generally be assumed to be 0.2 (Chen et al., 2011; Nakagaki et al., 2019). Furthermore, eNRTL uses the van't Hoff equation, shown in equation 14, for enthalpy change calculation. The heat of CO_2 absorption should take into account the enthalpy changes of all involved reactions, and therefore should be summed (Nakagaki et al., 2019) as shown in equation 15.

$$\frac{d(lnK_i)}{d\left(\frac{1}{T}\right)} = -\frac{\Delta H_{r,i}}{R} \quad (14)$$

$$\Delta H_r = \frac{\sum_i \left(\Delta n_i \Delta H_{r,i}\right)}{\Delta n_{CO_2}} \quad (15)$$

Furthermore, solubility can be expressed by Henry's law in equation 16:

$$P * y_{CO_2} * \phi_{CO_2} = H_{CO_2} * x_{CO_2} * \gamma^*_{CO_2} \quad (16)$$

where P is the pressure of the system, y_{CO_2} is the CO_2 mole fraction in the vapour phase, H_{CO_2} is the Henry's law constant of CO_2 in a water-amine matrix, x_{CO_2} is the CO_2 fraction in the liquid phase and $\gamma^*_{CO_2}$ is the unsymmetric activity coefficient of CO_2 in a water-amine solution. Henry's constant in the mixed solution can be calculated from pure solvents as shown in equation 17:

$$\ln\left(\frac{H_i}{\gamma_i^{\infty}}\right) = \sum_A w_A * \ln\left(\frac{H_{iA}}{\gamma_{iA}^{\infty}}\right) \tag{17}$$

where H_i is the Henry's constant of molecular solute i, such as CO_2 in the mixed solvent, H_{iA} is the Henry's constant of molecular solute i in pure solvent A, γ_i^{∞} is the infinite dilution activity coefficient of molecular solute i in the mixed solvent, γ_{iA}^{∞} is the infinite dilution activity coefficient of molecular solute i in pure solvent A and w_A is the weighting factor, which can be calculated by equation 18.

$$w_A = \frac{x_A (V_{iA}^{\infty})^{\frac{2}{3}}}{\sum_B x_B \left(V_{iB}^{\infty}\right)^{\frac{2}{3}}} \tag{18}$$

where x_A is the mole fraction of solvent A on solute-free basis and V_{iA}^{∞} is the partial molar volume of molecular solute i at infinite dilution in pure solvent A. Henry's constant for CO_2 in MEA gets the following expression in the study of Chen et al. (2011), presented in equation 19.

$$H_{CO_2,MEA}\,(Pa) = 6.6434 * 10^8 * \mathrm{e}^{\frac{-896.5}{\mathrm{T}}} \tag{19}$$

Finally, the general SRK EOS is defined by equation 20.

$$p = \frac{RT}{V_m - b} - \frac{a}{\sqrt{T} * V_m(V_m + b)} \tag{20}$$

where p is pressure, R is the universal gas constant, T is temperature, V_m is the molar volume, and a and b are model parameters that can be calculated from the gas critical point data.

5. Applied part

Based on the literature review, the goal of the applied part is to compare MEA and MDEA processes with the hot carbonate process. This is achieved by simulating separation processes for each of the steps to achieve the desired end goal of C2-C4 hydrocarbons. The construction of the model began with the MEA process. The simulations are done with the Aspen Plus V12.1 simulator.

The modelling was done in steady state/equilibrium approach to obtain mass and energy flows. This was seen adequate. However, it is acknowledged that a rate-based model with reaction kinetics and models accounting for mass transfer in the column packing could give more detailed information on the equipment sizing aspects.

The first step was defining all the present components in the Aspen Component Specification sheet. The component list is shown in Figure 10 and the present components were also mentioned earlier on in the literature review (see for example section 2. Properties of Fischer-Tropsch gases). The composition of the feed from Fischer-Tropsch synthesis is shown in Table 6. Figure 3 in the literature review section 2. Properties of Fischer-Tropsch gases shows the process steps and their order.

Table 6. The composition of the feed from Fischer-Tropsch synthesis.

Component	Feed kmol/hr	Feed mol-%
H2O	310.07	0.307
H2	288.36	0.285
CO2	139.30	0.138
CO	148.09	0.146
METHANE	18.12	0.018
ETHANE	3.90	0.004
PROPANE	5.20	0.005
BUTANE	4.42	0.004
PENTANE	0.06	0.000
HEXANE	0.02	0.000
ETHYLENE	49.77	0.049
BUTYLENE	15.59	0.015
PENTENE	3.14	0.003
PROPYLEN	13.69	0.014
HEXENE	1.58	0.002
HEPTENE	1.76	0.002
OCTENE	0.17	0.000
METOH	4.30	0.004
ETOH	1.59	0.002
PROPOH	0.74	0.001
BUTOH	0.34	0.000
PENTOH	0.13	0.000
ACETACID	0.89	0.001
PROPACID	0.33	0.000
BUTACID	0.10	0.000
TOTAL	1011.65	1

Component ID	Type	Component name	Alias	CAS number
H2O	Conventional	WATER	H2O	7732-18-5
H2	Conventional	HYDROGEN	H2	1333-74-0
CO2	Conventional	CARBON-DIOXIDE	CO2	124-38-9
CO	Conventional	CARBON-MONOXIDE	CO	630-08-0
METHANE	Conventional	METHANE	CH4	74-82-8
ETHANE	Conventional	ETHANE	C2H6	74-84-0
PROPANE	Conventional	PROPANE	C3H8	74-98-6
BUTANE	Conventional	N-BUTANE	C4H10-1	106-97-8
PENTANE	Conventional	N-PENTANE	C5H12-1	109-66-0
HEXANE	Conventional	N-HEXANE	C6H14-1	110-54-3
ETHYLENE	Conventional	ETHYLENE	C2H4	74-85-1
BUTYLENE	Conventional	1-BUTENE	C4H8-1	106-98-9
PENTENE	Conventional	1-PENTENE	C5H10-2	109-67-1
PROPYLEN	Conventional	PROPYLENE	C3H6-2	115-07-1
HEXENE	Conventional	1-HEXENE	C6H12-3	592-41-6
HEPTENE	Conventional	1-HEPTENE	C7H14-7	592-76-7
OCTENE	Conventional	1-OCTENE	C8H16-16	111-66-0
METOH	Conventional	METHANOL	CH4O	67-56-1
ETOH	Conventional	ETHANOL	C2H6O-2	64-17-5
PROPOH	Conventional	1-PROPANOL	C3H8O-1	71-23-8
BUTOH	Conventional	N-BUTANOL	C4H10O-1	71-36-3
PENTOH	Conventional	1-PENTANOL	C5H12O-1	71-41-0
ACETACID	Conventional	ACETIC-ACID	C2H4O2-1	64-19-7
PROPACID	Conventional	PROPIONIC-ACID	C3H6O2-1	79-09-4
BUTACID	Conventional	N-BUTYRIC-ACID	C4H8O2-1	107-92-6
MEA	Conventional	MONOETHANOLAMINE	C2H7NO	141-43-5
MEA+	Conventional	MEA+	C2H8NO+	
H3O+	Conventional	H3O+	H3O+	
MEACOO-	Conventional	MEACOO-	C3H6NO3-	
OH-	Conventional	OH-	OH-	
HCO3-	Conventional	HCO3-	HCO3-	
CO3--	Conventional	CO3--	CO3-2	

Figure 10. List of components in the simulated process in Aspen Plus V12.1.

As can be seen from Figure 10, the system contains a large number of components. Therefore, several process steps are required to separate them from each other, especially as some of them are known to be difficult to be separated from each other.

The initial idea for modelling was taken from May et al. (2012), where it was shown that water and heavier hydrocarbons could be separated by flashing. The purpose of the first process step is to separate water, alcohols, and acids from the system so that the next step of separating heavier hydrocarbons would not contain too many impurities. It is also important to eliminate the forming of azeotropes further on in the process, as a mixture of water, alcohols and acids has a tendency to form azeotropes.

The initial flowsheet for the first two process steps is shown in Figure 11. In the figure, the stream FEED is the stream from Fischer-Tropsch synthesis with the composition of Table 6. The other streams are named by what they contain, water phase as WATER, hydrocarbon phase as HYDCARBS and gaseous phase as GAS. The name COMPGAS is just the compressed gaseous phase. Stream LHC contains light hydrocarbons and other light gases, while the HHC phase is heavier hydrocarbons.

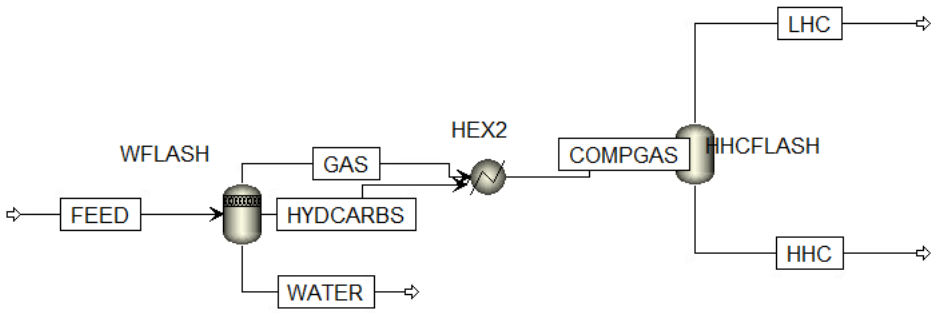

Figure 11. Initial flowsheet for the separation of water and heavier hydrocarbons from the mixture.

In the system, a 3-phase flash was chosen due to the VLL-equilibrium found between water and alcohols and acids in the NIST experimental database (Othmer et al., 1941 and Ochi et al., 1990). For the separation of water, the cubic plus association (CPA) method was chosen due to the best performance considering the solubilities of hydrocarbons in water (PubChem, 2023). Additionally, in the analysis done with Aspen, the estimated datapoints matched relatively well to experimental data. The initial process conditions for building the model for water separation were chosen to be 20 bars and 0 C. Therefore, some of the heavier hydrocarbons also went into the water phase. Furthermore, as the second liquid phase (HYDCARBS) from Figure 11 contained mostly hydrocarbons, it was fed to the heavy hydrocarbon flash along with the gas phase.

The conditions chosen for heavy hydrocarbon separation were 30 bars and 0 C, as either temperature must be decreased, or pressure must be increased for further heavy hydrocarbon separation. The conditions were set with heat exchanger HEX2 (Figure 11), using the SRK model, so the least number of thermodynamical

inconsistencies between methods would be present further in the simulation process, as the absorber and stripper are going to be run on eNRTL-RK. The SRK-method is the most commonly used method for hydrocarbons in elevated pressures along with Peng-Robinson. When simulated, even with modifications, too much of pentane exits as the distillate with light gases in terms of the desired product. This led to changing the process somewhat, as shown in Figure 12.

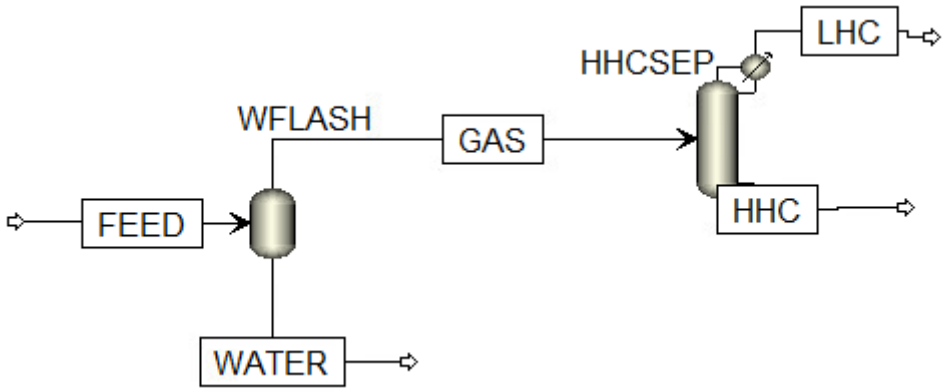

Figure 12. Flowsheet for water and heavy hydrocarbon separation after changes.

In the system in Figure 12, the water flash was set to operate in 15 bars and 10 C, as it was seen more economical to operate compared to 0 C and 20 bars, as maintaining 0 C is more energy intensive, and the difference in separation is minimal. Furthermore, as the absorber later on will be in atmospheric pressure, less decompression will be required. 3-phase flash was also switched back to 2-phase, as separating 3 different phases in a continuous process with a high feed rate could be difficult. Furthermore, the second liquid phase obtained in the 3-phase simulation in Figure 11 contained mainly hydrocarbons, which would have been fed to the heavy hydrocarbon separation in any case.

Heavy hydrocarbon separation was changed from flash to distillation due to inadequate separation. Here the C2-C4 hydrocarbons need to be conserved in contrary to natural gas processing, where flashing is sufficient due to only needing to conserve methane, as shown in the study by May et al. (2012). The reflux ratio was set to 5 to achieve a satisfactory separation along with 25 stages to make the column tall enough for separation to take place. Finally, the amount of light hydrocarbons and

other light gases was calculated to be 686 kmol/hr, which was then set to be the distillate rate, which makes Aspen calculate duties for the reboiler and the condenser. The distillation column is also set to operate at 15 bars to eliminate the need for excessive compressing or decompressing between following process steps.

After the separation of heavier hydrocarbons and water, the remaining CO_2 must be separated from the lighter hydrocarbon stream. This is done in a typical absorber-stripper system, similarly as in Figure 5. Initially the simulation was run without recycling of amine to get an understanding of how sensitive the system is to changes and if it converges as a standalone system. The initial flowsheet for the absorber-stripper system is shown in Figure 13.

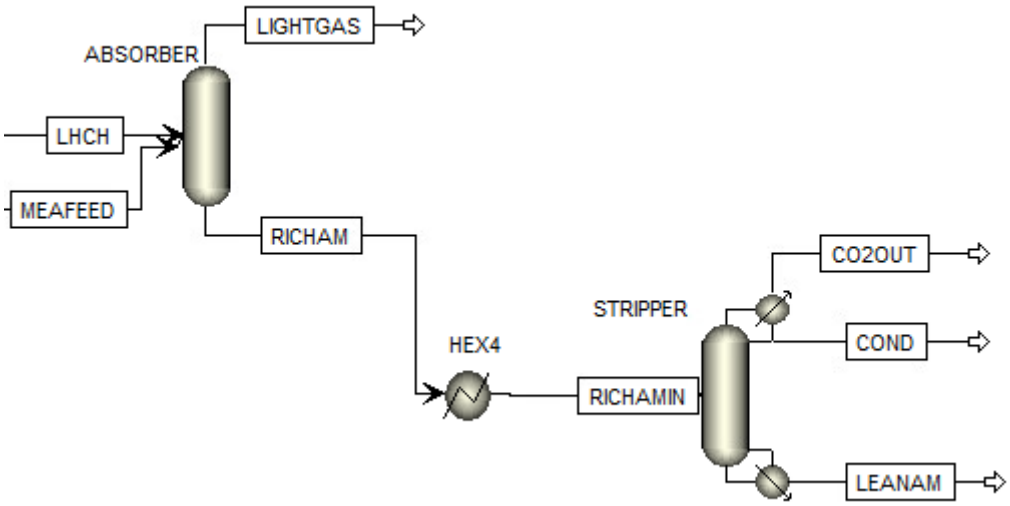

Figure 13. The initial absorber-stripper system.

The pressure chosen for the absorber and stripper were 1 and 2 bars, respectively. These were chosen based on the MEA eNRTL-RK template model in Aspen Plus V12.1 after higher pressures were tested without success, as the simulations did not converge, although the study of Shahid et al. (2019) shows that the system should be operatable and even more efficient at higher pressures, as the partial pressure of CO_2 rises, making absorption more efficient.

For this part of the process, the reactions between MEA, CO_2 and H_2O must be specified. Therefore, with Aspen Plus V12.1 electrolyte wizard and eNRTL package the reactions were automatically generated. These reactions as shown in Figure 14.

	Reaction	Type	Stoichiometry	Delete
▶	1	Equilibrium	H2O + MEACOO- <--> MEA + HCO3-	✕
▶	2	Equilibrium	H2O + HCO3- <--> CO3-- + H3O+	✕
▶	3	Equilibrium	2 H2O + CO2 <--> HCO3- + H3O+	✕
▶	4	Equilibrium	2 H2O <--> OH- + H3O+	✕
▶	5	Equilibrium	H2O + MEA+ <--> MEA + H3O+	✕

Figure 14. The reactions between MEA, CO_2 and H_2O.

The reactions match those of Chen et al (2011) and the equilibrium constants for each reaction were automatically retrieved from Aspen databanks. Furthermore, to help with proper convergence, non-condensable components can be identified as Henry components in the Aspen specification sheet. In this case, CO_2, CO, H_2 and methane are non-condensable, therefore they are specified as Henry components. Additionally, as ethane and ethylene's critical points are at 32.2 and 9.2 °C respectively (EngineeringToolBox, 2008, and 2018), they should also be added to the Henry component list, but this caused Aspen to continuously crash and therefore they have been left out. Thus, Aspen searches for Henry constants from the databank APV121 HENRY-AP for every existing binary pair. Furthermore, as eNRTL-RK is chosen as the method, Aspen automatically retrieves data for the binary pairs from the databanks APV121 LLE-ASPEN, APV121 VLE-RK and NISTV121 NIST-RK.

The initial value for MEA feed into the absorption column was taken from the study of May et al. (2012), where it was mentioned that MEA can absorb 0.5 moles of CO_2 per mole of MEA. Furthermore, it is mentioned by Akram et al. (2020) that the most commonly used weight distribution is 70% water and 30% MEA, as it is the in-between solution of not being too corrosive but exhibiting decent energy consumption rates. However, this caused convergence problems, and thus a solution of 85% water and 15% MEA was chosen instead, while maintaining the initial ratio of approximately 2:1 MEA:CO_2. Thus, the amount of feed was 5800 kmol/hr.

However, when simulating the absorber-stripper system, it was found out that Aspen did not have NRTL parameters for the interaction between water and ethane/ethylene as well as water and butane/butylene. Therefore, they had to be regressed from experimental data. Numerous datapoints from the studies of Bradbury et al. (1952), Davis & McKetta (1960), Tsiklis et al. (1960), Mcauliffe (1966), Anthony & McKetta (1967), and Sanchez & Lentz (1973) were retrieved from the NIST database and used in the regression between water and ethylene. The used method for regression analysis was eNRTL-RK, as chosen for the absorber-stripper process step. A demonstration of a regression analysis is shown in Figures 15 and 16.

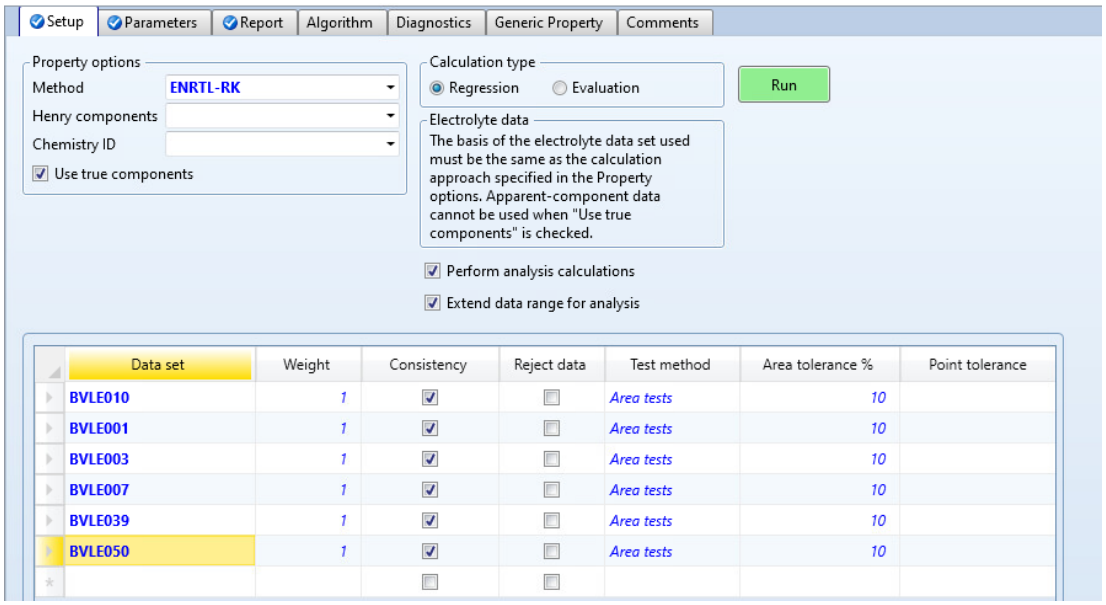

Figure 15. Example of a regression analysis Setup screen.

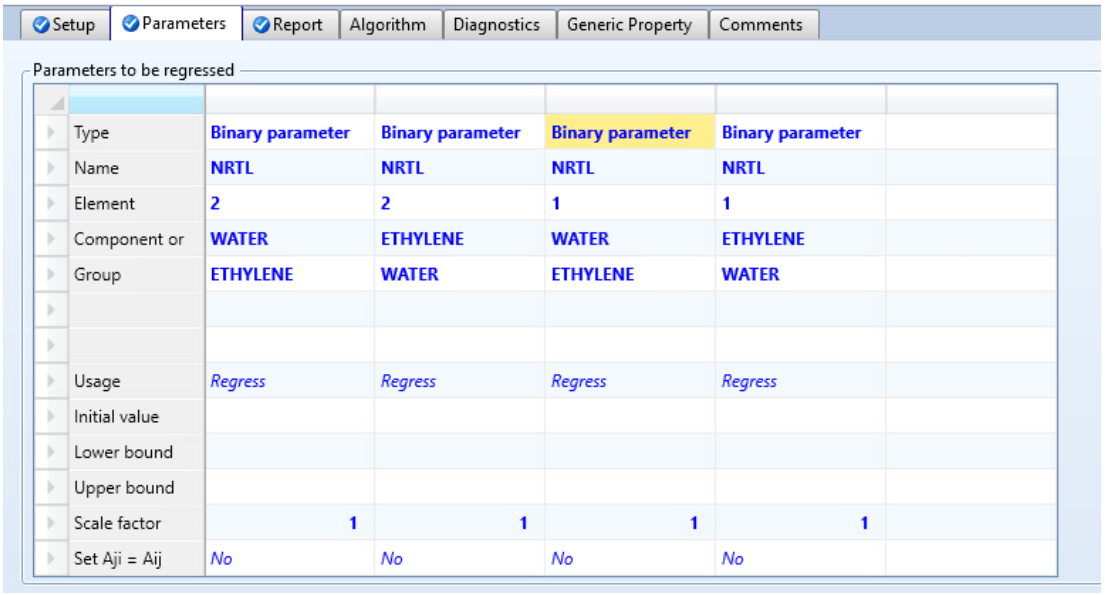

Type	Binary parameter	Binary parameter	Binary parameter	Binary parameter
Name	NRTL	NRTL	NRTL	NRTL
Element	2	2	1	1
Component or	WATER	ETHYLENE	WATER	ETHYLENE
Group	ETHYLENE	WATER	ETHYLENE	WATER
Usage	*Regress*	*Regress*	*Regress*	*Regress*
Initial value				
Lower bound				
Upper bound				
Scale factor	1	1	1	1
Set Aji = Aij	*No*	*No*	*No*	*No*

Figure 16. Example of a regression analysis Parameters tab.

In the Setup screen, all the chosen datasets are selected for regression and then on the Parameters tab, the relevant parameters are chosen to be regressed. In this case, the NRTL interaction parameters between water and ethylene need to be optimised, and the first 2 elements determine their interaction as they are the activity coefficients. The same was done for water-ethane, water-butane, and water-butylene systems as well, but they did not have enough experimental datasets to achieve relevant results and therefore the regressed values of ethylene were used for all the systems, as their behaviour is quite similar apart from the fact that butane is slightly less, and butylene is slightly more soluble in water (PubChem, 2023).

Another important notice was the fact that in the Pure Components tab REVIEW-1, formation energies for the MEA-ions were not automatically obtained, so they were taken from an Aspen Plus V12.1 template, in which the values were derived from numerous studies, such as Hilliard's (2008).

After these changes, the simulation converged again. This led to further development of the model with the addition of water separation after the absorber (WFLASH2) and cryogenic distillation (CRYODIST) as shown in the flowsheet in Figure 17, while each of the blocks, their operating conditions and function is shown in Table 7.

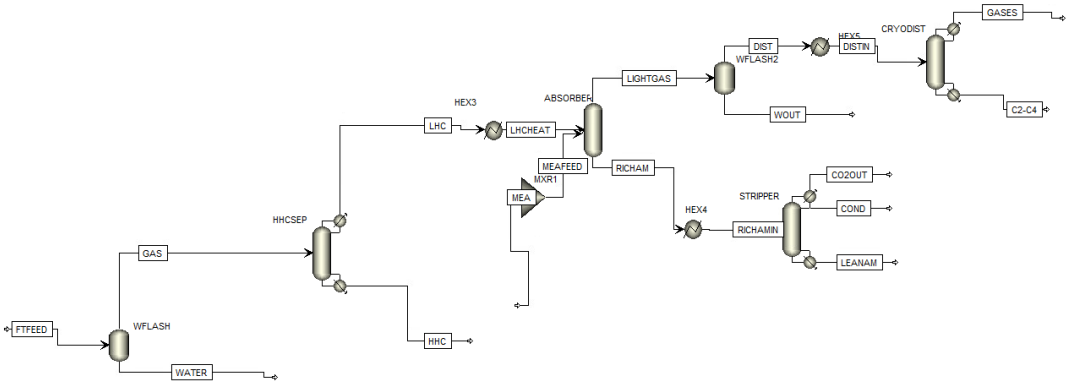

Figure 17. Once-through process flowsheet of the MEA model.

Table 7. Blocks in Aspen Plus V12.1 simulator, their operating conditions and their function.

Block/Aspen model	Operating conditions	Function
WFLASH Flash2	Temperature: 10 C Pressure: 15 bar Vapour-liquid equilibrium	Flash to separate water, alcohols and acids from the mixture.
HHCSEP Radfrac	25 stages Condenser: Partial-vapour Reboiler: Kettle Valid phases: Vapour-liquid Convergence: Petroleum/Wide-boiling[1] Distillate rate: 686 kmol/hr[2] Reflux ratio: 5 Product streams: LHC leaving from stage 1 as vapour, HHC from stage 25 as liquid. Inlet stream: GAS to stage 13.	Distilliation to separate and recycle heavier hydrocarbons from the mixture to make CO2-separation easier.
HEX3 Heater	Temperature: 45 C Pressure: 2 bar	To lower the pressure from 15 bar to 2 bar for more optimal feed pressure.
MXR1 Mixer	-	To mix make-up stream and the recycled lean amine stream later on; pre-emptively added block
ABSORBER Radfrac	20 stages, Pressure: 1 bar No condenser or reboiler Convergence: Custom (damping level set to medium from	Absorber to absorb the CO_2 with amine from the LHCHEAT stream to produce a CO_2-free LIGHTGAS stream for

	Convergence > Basic > Methods > Damping level) Feed streams: LHCHEAT to stage 20, MEAFEED to stage 1 Product streams: RICHAM from stage 20, LIGHTGAS from stage 1. Estimates[3]: Stage 1 temperature: 49 C Stage 20 temperature: 60 C Stage 12 temperature: 85 C	easier cryogenic distillation.
HEX4 Heater	Temperature: 112 C Pressure: 2 bar	To heat up the stream for better regeneration of MEA in the stripper.
STRIPPER Radfrac	25 stages, Condenser: Partial-vapour-liquid Reboiler: Kettle Valid phases: Vapour-liquid Convergence: Standard Reflux ratio: 5 Bottoms rate: 5500 kmol/hr[4] Feed stream: RICHAMIN to stage 3 Product streams: CO2OUT from stage 1 as vapour, COND from stage 1 as liquid, and LEANAM from stage 25 as liquid. Condenser pressure: 2 bar	To regenerate most of MEA for recycling purposes and capture of CO_2.
WFLASH2 Flash2	Temperature: 5 C Pressure: 15 bar	To separate most of the water from LIGHTGAS in order to prevent cryogenic distillation from freezing
HEX5 Heater	Temperature: -114 C Pressure: 40 bar	Cooling and compressing the light gas feed to match cryogenic

		distillation temperature (Kim & Do, 2020).
CRYODIST Radfrac	20 stages, Condenser: Partial-vapour Reboiler: Kettle Valid phases: Vapour-liquid Reflux ratio: 2 Bottoms to feed ratio: 0.166[5] Feed streams: Distin on stage 1 Product streams: Gases from stage 1 as vapour, C2-C4 from stage 20 as liquid. Condenser pressure: 40 bar	To liquefy the C2-C4 hydrocarbons in order to recycle H_2, methane and carbon monoxide back into catalytic partial oxidation and Fischer Tropsch synthesis and to acquire the desired end product.

[1] Did not converge in 200 iterations with standard convergence, so it was changed to Petroleum/Wide-boiling, as a large number of hydrocarbons are present and that helped with convergence.
[2] Calculated as an estimate of distillate when optimal separation occurs.
[3] Estimates are assumed in order to help with convergence on the basis of non-converging simulations and the study of Moioli et al. (2012).
[4] Bottoms rate calculated in a manner to help the stripper converge towards lean loading of ~25% as mentioned in the study of Choi et al (2019).
[5] Bottoms to feed ratio calculated in a manner to direct C2-C4 hydrocarbons towards the bottom and other gases towards the distillate.

After several steps mentioned above to get the simulation to converge as a once-through process, the aim was to recycle the lean amine back into the absorber. The initial idea was to connect the lean amine stream into a mixer where the recycled lean amine and make-up streams for water and MEA are mixed and then create design specs for the make-up streams of water and MEA to account for the losses in mid-process. The flowsheet of this idea of closing the loop is shown in Figure 18, while the water and MEA make-up design specs are shown in Figures 19-21.

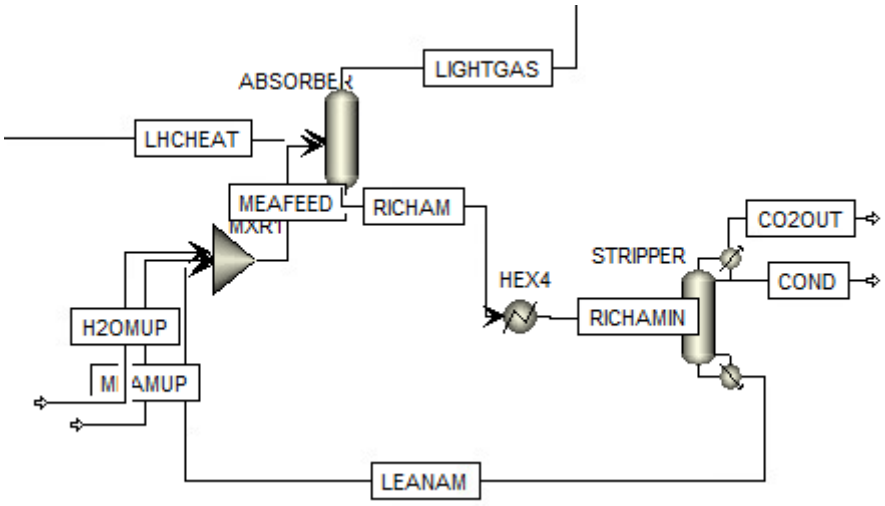

Figure 18. Flowsheet of the absorber-stripper system with a closed recycling loop.

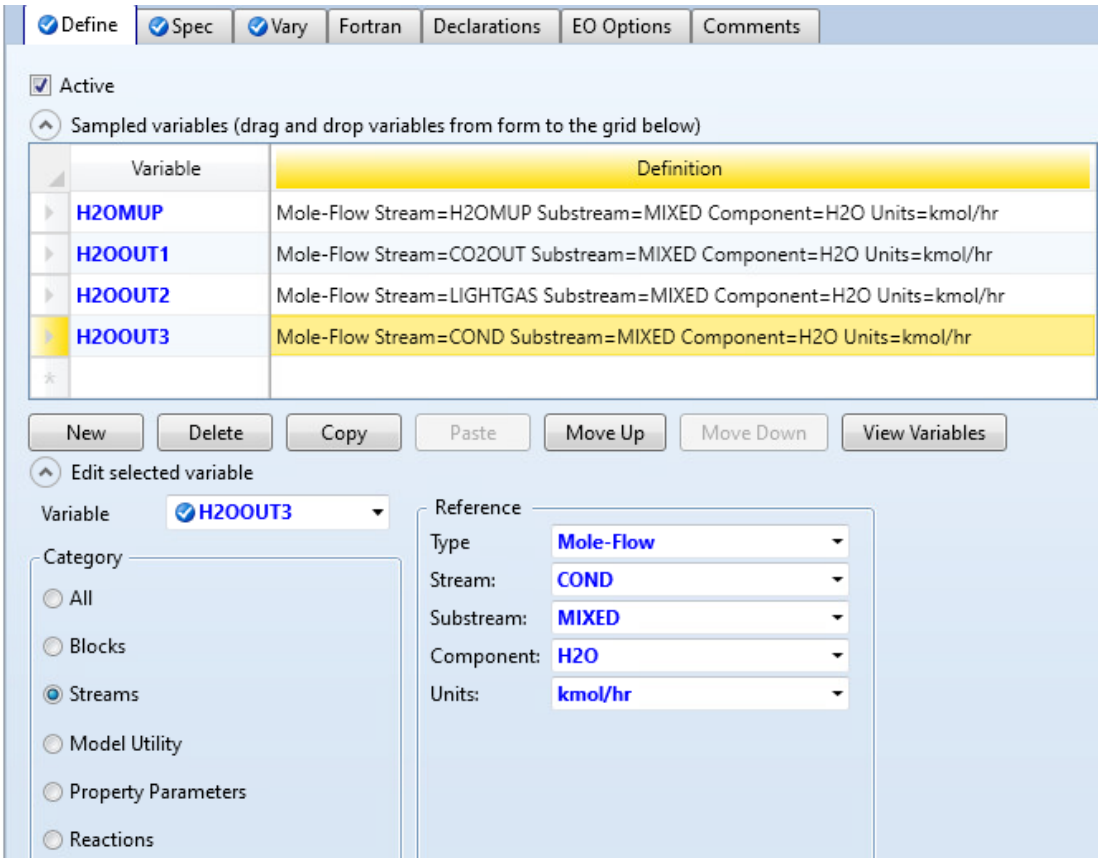

Figure 19. Water make-up specifications.

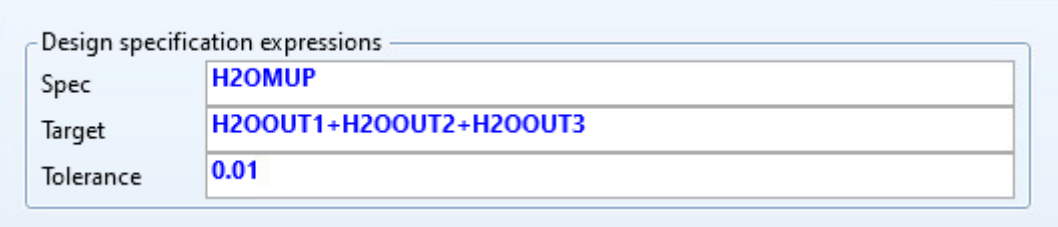

Figure 20. Water make-up specifications.

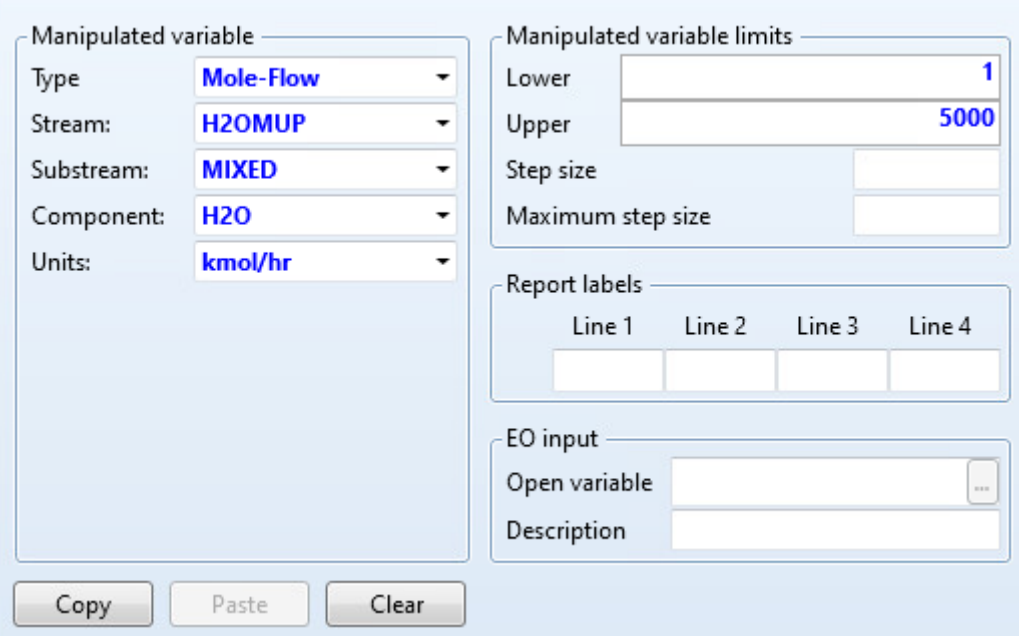

Figure 21. Water make-up stream manipulated variable.

In Figure 19, the variables are defined as the water make-up stream (H2OMUP) and water exits (H2OOUT1-3), which resemble the water exiting through LIGHTGAS, CO2OUT and COND streams, respectively. Figure 20 shows that the make-up stream for water is to match the sum of the exiting streams, and Figure 21 shows that the stream H2OMUP is being manipulated to achieve the target. The same process was done for the MEA make-up design spec, but the simulation failed to converge, calling for more changes.

The next idea to promote convergence was to use a splitter to control the amount of lean amine that is being recycled to slowly accommodate the absorber towards full recycling, the idea shown in Figure 22.

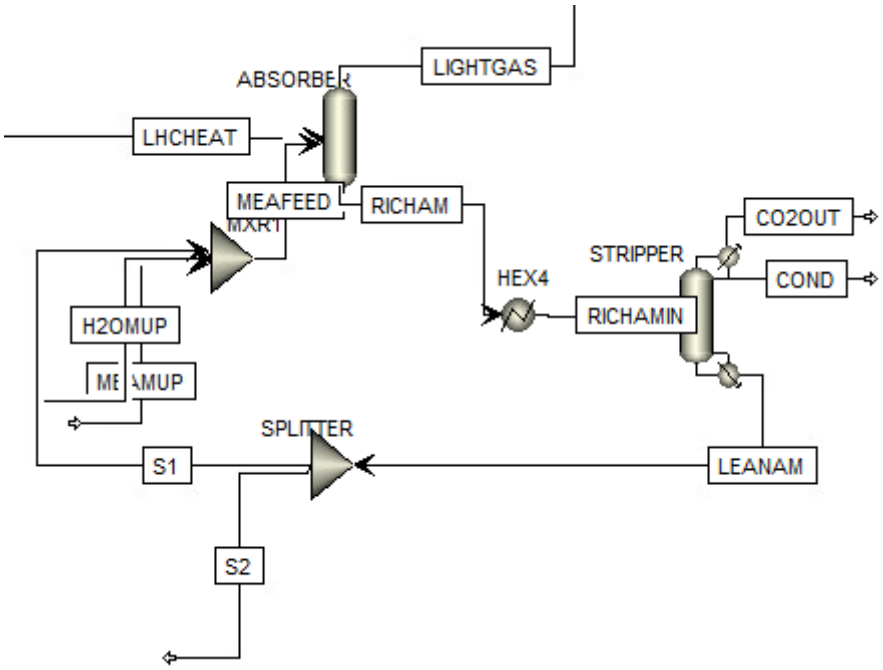

Figure 22. Flowsheet with a splitter to control the amount of LEANAM recycling to the absorber.

However, even with this change, the absorber still failed to converge. There was a forum post on Researchgate by prof. Penteado suggesting setting a content of CO_2 in the lean stream to initialise the simulation (Researchgate, 2015), so it was decided to give up on a closed loop, but rather use design specs to close the recycling, the flowsheet is shown in Figure 23.

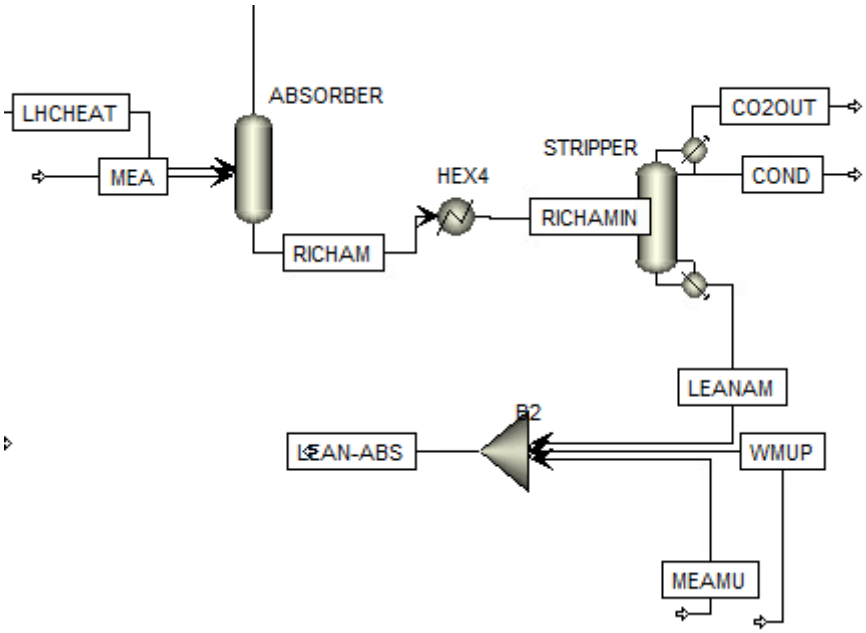

Figure 23. Flowsheet of the process, where design specs are used to close the recycling.

In Figure 23, the idea is to use a design spec in Aspen to match the streams MEA and LEAN-ABS which consists of the streams LEANAM (bottoms of the stripper) and make-up streams of water and MEA, WMUP and MEAMU, respectively. Further details of the specifications are given below. Here, in the initial feed (MEA), the composition of the feed has been changed slightly from the once-through process. Now, as mentioned by prof. Penteado, a 0.5 w-% fraction of CO_2 has been added to the feed to help with convergence, while the w-% of MEA is 17 and water is 82.5. The design specs have also been modified on the basis of the once-through conversion. The design specs for the recycling are presented in Figures 24-32.

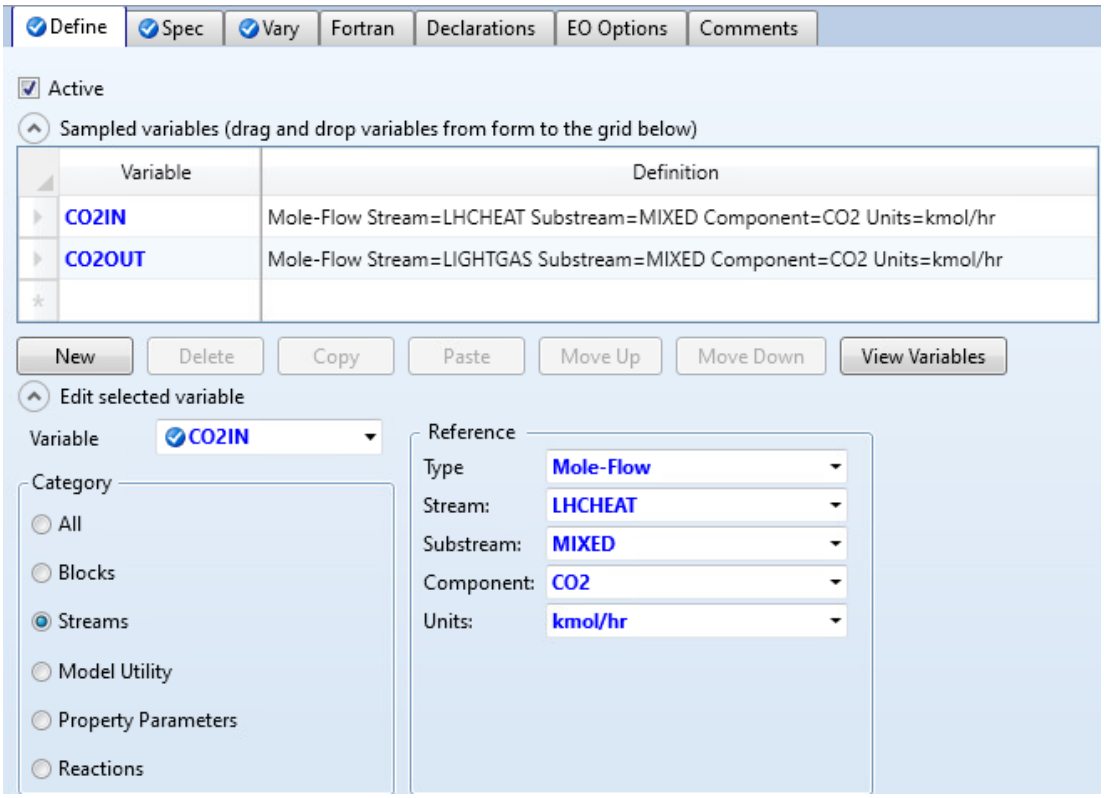

Figure 24. Design spec for CO_2 exiting with light gases from the absorber.

Figure 25. Design spec specifying that 1% of entering CO_2 from FT exits with light gases from the absorber.

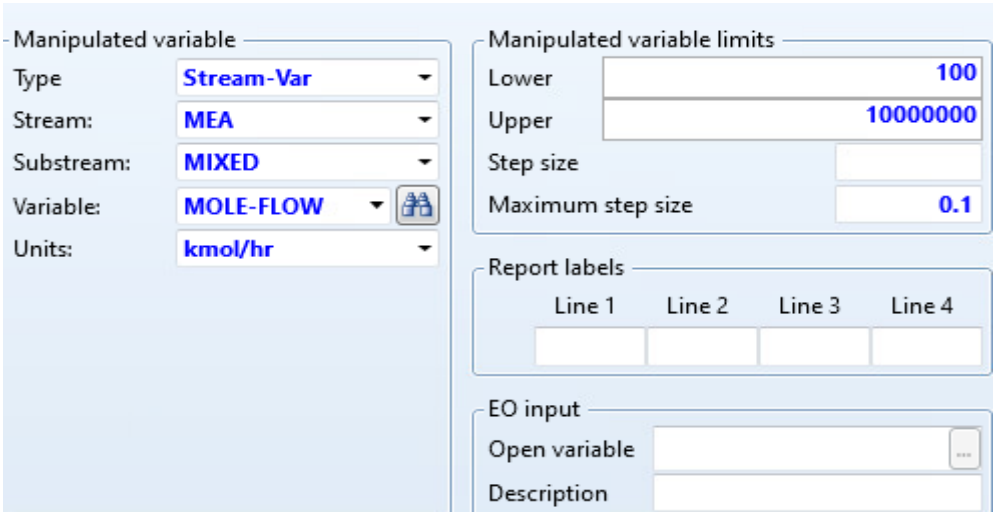

Figure 26. Design spec specifying that the molar flow rate of the stream MEA is being varied to accomplish the target.

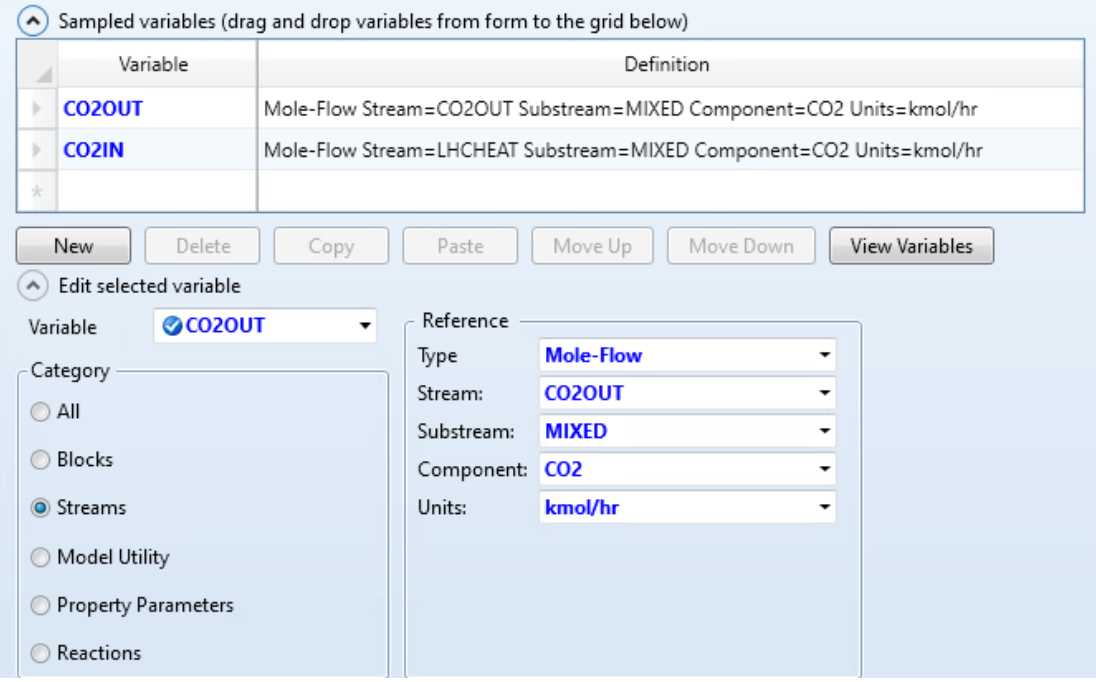

Figure 27. Design spec for CO_2 exiting through CO2OUT stream from the stripper.

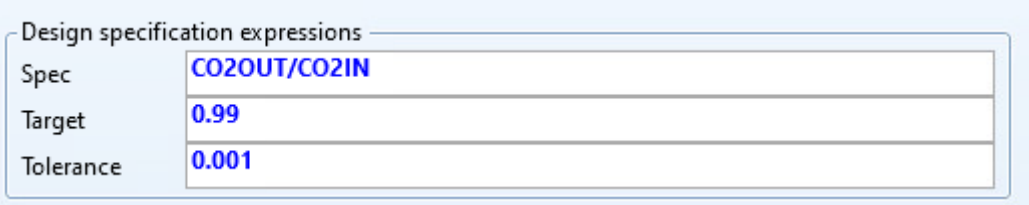

Figure 28. Design spec specifying that 99% of entering CO_2 from FT exits from the distillate stream of the stripper.

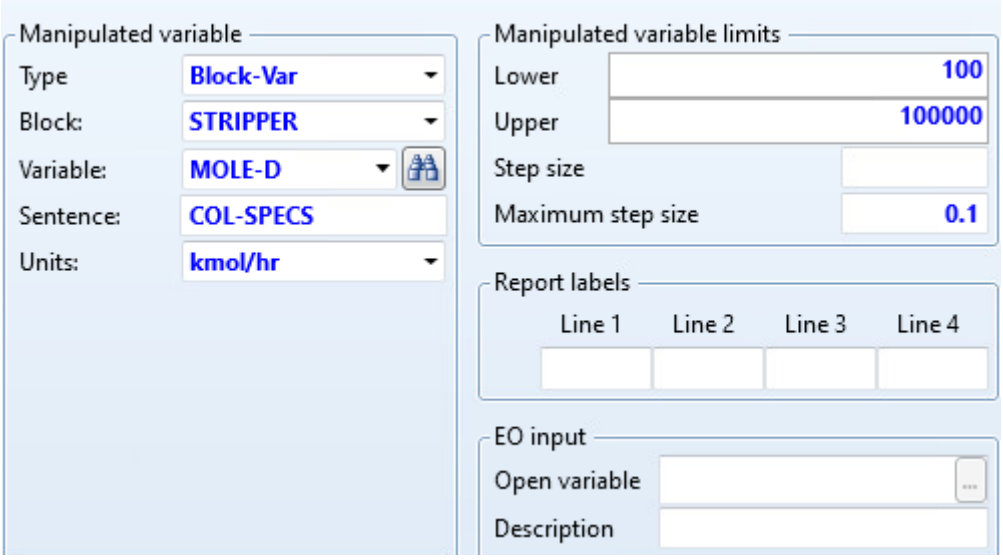

Figure 29. Design spec specifying that the molar flow rate of the distillate stream of the stripper is being varied to accomplish the target.

MEA make-up stream is specified similarly to Figures 19-21, but now the water make-up stream is specified differently to achieve a loop that resembles recycling.

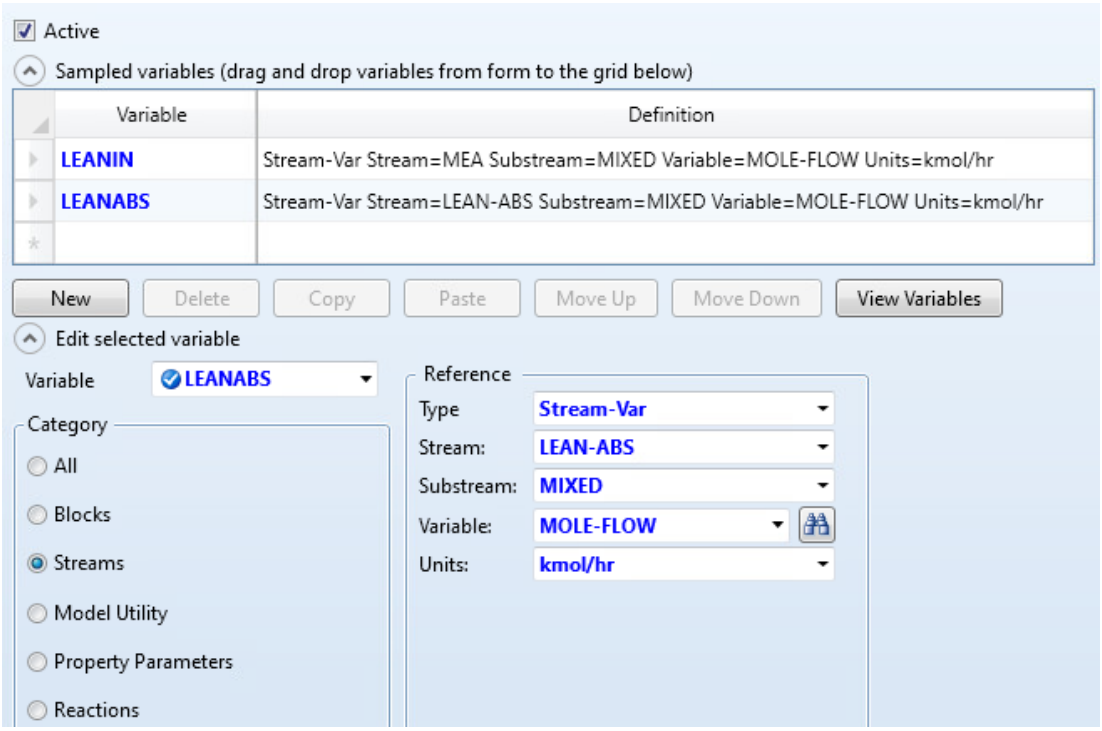

Figure 30. Design spec for recycling the lean amine.

Figure 31. Design spec specifying that the molar flow rates of the streams LEANIN and LEANABS should be equal.

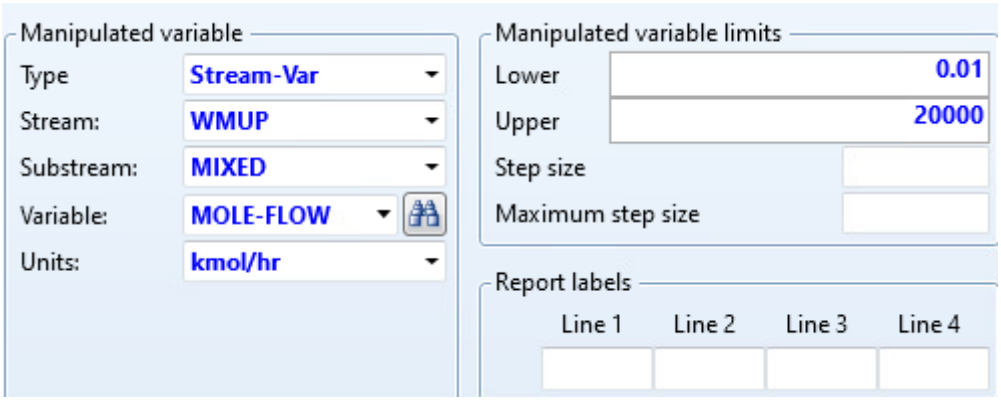

Figure 32. Design spec specifying that the mole flow of stream WMUP is being varied to achieve the target.

The goal of the design spec presented in Figures 30-32 is to specify that the stream molarity of MEA matches the stream molarity of LEAN-ABS in Figure 23, and the stream WMUP is the varied factor to make that happen. Furthermore, the CO_2 that is initially fed in through the stream MEA, is set to circle around in the process through the design specs shown in Figures 24-32, as it is assumed that only the CO_2 from Fischer-Tropsch synthesis is captured from the stripper. Furthermore, in this model, the specification of feed to bottoms ratio of the cryogenic distillation was changed to bottoms rate, which was calculated to be around the sum of C2-C4 paraffins and olefins to help with convergence.

Furthermore, some studies, such as the one by Ahn et al. (2013), suggest that a water loop could be installed on top of the absorber to cool it down, while also working as an amine wash for the exiting stream. This idea was tried out as shown in Figure 33.

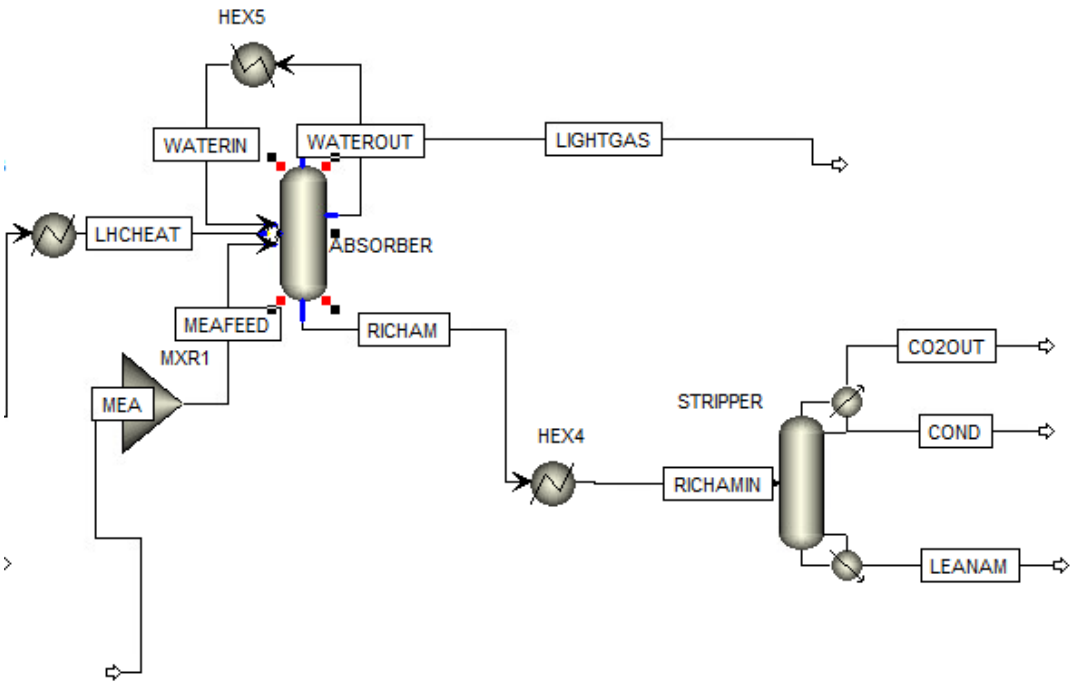

Figure 33. Absorber-stripper system with water pump around at the top of the absorber.

In the system, MEAFEED is then fed to stage 3 instead of stage 1, while the water recycling now enters at stage 1 and exits from stage 2. LHCHEAT still enters on stage 20 and RICHAM exits from stage 20 as well. However, with any modifications to feed stages or amounts in this model, the simulation would not converge with a water loop.

Finally, in the working models shown in Figures 17 and 23, the kinetics for the reactions were tried out to compare the differences in results. The kinetic reactions are presented in Aspen as shown in Figure 34, and they are entered in the Reactions tab in the Simulation sheet.

Rxn No.	Reaction type	Stoichiometry	Delete
1	EQUIL	MEAH+ + H2O <--> MEA + H3O+	✕
2	EQUIL	2.0 H2O <--> H3O+ + OH-	✕
3	EQUIL	HCO3- + H2O <--> CO3-2 + H3O+	✕
4	KINETIC	OH- + CO2 --> HCO3-	✕
5	KINETIC	HCO3- --> OH- + CO2	✕
6	KINETIC	MEA + CO2 + H2O --> MEACOO- + H3O+	✕
7	KINETIC	MEACOO- + H3O+ --> MEA + CO2 + H2O	✕

Figure 34. The reactions of the MEA-CO_2-H_2O system.

The kinetic parameters for the built-in power law were taken and derived from the studies of Pinsent et al. (1956) and Hikita et al. (1977). The power law is presented in Equation 21 and the parameter values are presented in Table 8.

$$r = kT^n e^{-\frac{E}{RT}} \prod_{i=1}^{N} (x_i \gamma_i)^{a_i} \tag{21}$$

Where r is the rate of reaction, T is the temperature, n is the temperature exponent, E is the activation energy, R is the universal gas constant, N is the number of components in the reaction, x_i is the mole fraction of component *i*, γ_i is the activity coefficient of component *i,* and a_i is the stoichiometric coefficient of component *i* in the reaction equation.

Table 8. Parameters k and E in the built in power law.

Reaction number	k	E, cal/mol
4	1.33e+17	13249
5	6.63e+16	25656
6	3.02e+14	9855.8
7 (in absorber)	5.52e+23	16518
7 (in stripper)	6.50e+27	22782

The parameters for absorber and stripper are different, as they are operated in different temperature ranges. However, when entering the kinetics and the parameters in the simulation, it crashes and will not run.

For comparison, the MDEA and K_2CO_3 models are built using the MEA model as a template and therefore they do not differ much apart from the component listing. The component listings and reactions of MDEA and K_2CO_3 models are shown in Figures 35-38, from the parts that they start to differ from the one of the MEA model. The reactions are from Aspen Plus V12.1 electrolyte wizard, similarly to MEA model.

PROPACID	Conventional	PROPIONIC-ACID	C3H6O2-1	79-09-4
BUTACID	Conventional	N-BUTYRIC-ACID	C4H8O2-1	107-92-6
MDEA	Conventional	METHYL-DIETHANOLAMINE	C5H13NO2	105-59-9
MDEA+	Conventional	MDEA+	C5H14NO2+	
H3O+	Conventional	H3O+	H3O+	
OH-	Conventional	OH-	OH-	
HCO3-	Conventional	HCO3-	HCO3-	
CO3--	Conventional	CO3--	CO3-2	

Figure 35. The part of the component listing of the MDEA model that differs from the MEA model.

	Reaction	Type	Stoichiometry	Delete
1	Equilibrium	H2O + HCO3- <--> CO3-- + H3O+	✕
2	Equilibrium	2 H2O + CO2 <--> HCO3- + H3O+	✕
3	Equilibrium	H2O + MDEA+ <--> MDEA + H3O+	✕
4	Equilibrium	2 H2O <--> OH- + H3O+	✕

Figure 36. The reactions taking place in the MDEA model.

PROPACID	Conventional	PROPIONIC-ACID	C3H6O2-1	79-09-4
BUTACID	Conventional	N-BUTYRIC-ACID	C4H8O2-1	107-92-6
POTAS-01	Conventional	POTASSIUM-CARBONATE	K2CO3	584-08-7
K+	Conventional	K+	K+	
H3O+	Conventional	H3O+	H3O+	
OH-	Conventional	OH-	OH-	
HCO3-	Conventional	HCO3-	HCO3-	
CO3--	Conventional	CO3--	CO3-2	

Figure 37. The part of the component listing of the K_2CO_3 model that differs from the MEA model.

	Reaction	Type	Stoichiometry	Delete
	1	Equilibrium	H2O + HCO3- <--> CO3-- + H3O+	
	2	Equilibrium	2 H2O + CO2 <--> HCO3- + H3O+	
	KHCO3(S)	Salt	KHCO3(S) <--> HCO3- + K+	
	K2CO3(S)	Salt	K2CO3(S) <--> CO3-- + 2 K+	
▶	POTAS-01	Dissociation	POTAS-01 --> CO3-- + 2 K+	

Figure 38. The reactions taking place in the K_2CO_3 model.

For these models, connecting the recycle stream from the stripper to the absorber did not converge, so the flowsheets match Figure 17. For K_2CO_3 the absorber pressure was found out to differ from that of MEA, as potassium carbonate absorbers are run at lowest in 10 bar pressures and at highest in 120 C temperatures (Oil & Gas Process Engineering, 2018). Thus, the feed was fed in at 22 bars and 110 C, while the absorber pressure was at 20 bars. Different compositions of K_2CO_3-H_2O feed were tried out, but nothing relevant could be obtained from the simulation. In the MDEA-model, the conditions are the same as in the MEA model, the only difference is that the composition of the MDEA – H_2O mixture is 65 w-% H_2O and 35 w-% MDEA.

6. Results

Simulations were performed with each model, although more thoroughly with the MEA model, as it was the starting point. Although this chapter will mostly concentrate on the CO_2 separation step, with it being the focus of the thesis, some interesting results from the other steps will also be presented. The initial behaviour differences between eNRTL-RK and SRK models were compared within the heavy hydrocarbon separation, in the flash column. Figure 39 shows the results with e-NRTL and SRK models in the same conditions. The value (COMPGAS) on the left is the feed, the value in the middle (HHC) is the heavier hydrocarbon fraction, while the value on the right (LHC) is the lighter hydrocarbon fraction.

	Units	COMPGAS	HHC	LHC		Units	COMPGAS	HHC	LHC
Mole Flows	**kmol/hr**	**693.574**	**24.4099**	**669.164**	**Mole Flows**	**kmol/hr**	**693.574**	**20.1255**	**673.448**
H2O	kmol/hr	0.286376	0.28493	0.00144602	H2O	kmol/hr	0.286376	0.162521	0.123856
H2	kmol/hr	288.321	3.3689e-07	288.321	H2	kmol/hr	288.321	0.166123	288.155
CO2	kmol/hr	138.362	4.98154	133.38	CO2	kmol/hr	138.362	3.56765	134.794
CO	kmol/hr	148.06	0.695157	147.365	CO	kmol/hr	148.06	0.259544	147.8
METHANE	kmol/hr	18.1101	0.299311	17.8108	METHANE	kmol/hr	18.1101	0.0904409	18.0197
ETHANE	kmol/hr	3.89724	0.179382	3.71786	ETHANE	kmol/hr	3.89724	0.132078	3.76516
PROPANE	kmol/hr	5.19653	0.774611	4.42192	PROPANE	kmol/hr	5.19653	0.644744	4.55178
BUTANE	kmol/hr	4.42208	1.76426	2.65782	BUTANE	kmol/hr	4.42208	1.54087	2.88121
PENTANE	kmol/hr	0.0649045	0.0456307	0.0192738	PENTANE	kmol/hr	0.0649045	0.0432418	0.0216627
HEXANE	kmol/hr	0.0150949	0.013548	0.00154686	HEXANE	kmol/hr	0.0150949	0.0133072	0.00178768
ETHYLENE	kmol/hr	49.7665	1.63142	48.1351	ETHYLENE	kmol/hr	49.7665	1.03833	48.7282
BUTYLENE	kmol/hr	15.5907	5.56808	10.0226	BUTYLENE	kmol/hr	15.5907	4.8633	10.7274
PENTENE	kmol/hr	3.13828	2.06796	1.07032	PENTENE	kmol/hr	3.13828	1.90483	1.23345
PROPYLEN	kmol/hr	13.6893	1.72841	11.9609	PROPYLEN	kmol/hr	13.6893	1.38405	12.3053
HEXENE	kmol/hr	1.57652	1.38506	0.191466	HEXENE	kmol/hr	1.57652	1.35366	0.222866
HEPTENE	kmol/hr	1.76018	1.69115	0.0690295	HEPTENE	kmol/hr	1.76018	1.68517	0.0750058
OCTENE	kmol/hr	0.173889	0.172066	0.00182287	OCTENE	kmol/hr	0.173889	0.171723	0.00216624
METOH	kmol/hr	0.0855932	0.0772683	0.00832486	METOH	kmol/hr	0.0855932	0.0681404	0.0174527
ETOH	kmol/hr	0.122378	0.118721	0.00365648	ETOH	kmol/hr	0.122378	0.11229	0.0100878
PROPOH	kmol/hr	0.154628	0.153079	0.00154892	PROPOH	kmol/hr	0.154628	0.14989	0.00473803
BUTOH	kmol/hr	0.184803	0.184409	0.000394019	BUTOH	kmol/hr	0.184803	0.182842	0.00196144
PENTOH	kmol/hr	0.114499	0.114422	7.71481e-05	PENTOH	kmol/hr	0.114499	0.114072	0.000426301
ACETACID	kmol/hr	0.188661	0.187338	0.0013234	ACETACID	kmol/hr	0.188661	0.185058	0.00360393
PROPACID	kmol/hr	0.189798	0.18953	0.000268159	PROPACID	kmol/hr	0.189798	0.189013	0.000785277
BUTACID	kmol/hr	0.102678	0.102645	3.29892e-05	BUTACID	kmol/hr	0.102678	0.102586	9.27392e-05

Figure 39. Heavy hydrocarbon separation with eNRTL-RK and SRK.

The behaviour between water and ethylene with eNRTL-RK inside the absorber without regressed parameters is shown in Table 9.

Table 9. Water-ethylene behaviour without regressed NRTL parameters.

		LHCHEAT	RICHAM	LIGHTGAS
WATER	kmol/hr	5228	5189,72	38,2806
ETHYLENE	kmol/hr	49,5	26,8956	22,6044

Table 9 shows that ethylene is not separated well, as too much of ethylene is dissolving into water (PubChem, 2023) and therefore regression for the parameters

should be done. Once all the datasets were fed in as shown in Figures 15 and 16 and the analysis was run, the following results were obtained, as shown in Figure 40.

Regressed parameters

	Parameter	Component i	Component j	Value (SI units)	Standard deviation
▶	NRTL/2	WATER	ETHYLENE	-1165.92	505.95
	NRTL/2	ETHYLENE	WATER	3980.67	662.762
	NRTL/1	WATER	ETHYLENE	8.01567	1.55547
	NRTL/1	ETHYLENE	WATER	-8.92613	1.10918

Figure 40. NRTL parameter regression.

After plugging in these values for the NRTL binary parameters and simulating the system within the same conditions, the following results were obtained, as shown in Table 10.

Table 10. Water-ethylene behaviour with regressed NRTL-parameters.

		LHCHEAT	RICHAM	LIGHTGAS
WATER	kmol/hr	5228	5172,35	55,6494
ETHYLENE	kmol/hr	49,5	0,116314	49,3837

Table 10 shows much more promising results compared to Table 9. Initially, using parameters from the Aspen databank, the absorber-stripper system could not converge.

Once the NRTL parameters were regressed and the formation enthalpies of MEA ions were found and entered, also estimates were made for stage temperatures to help the column converge. This helped with forming the following temperature profile, as shown in Figure 41. Figure 42 shows the temperature profile in the finalized MEA model with recycling. For comparison purposes, 1 bar and 15 bar MDEA temperature profiles are also presented in Figures 43 and 44. The K_2CO_3 model never gave any reliable results due to convergence issues, therefore it is not in comparison here.

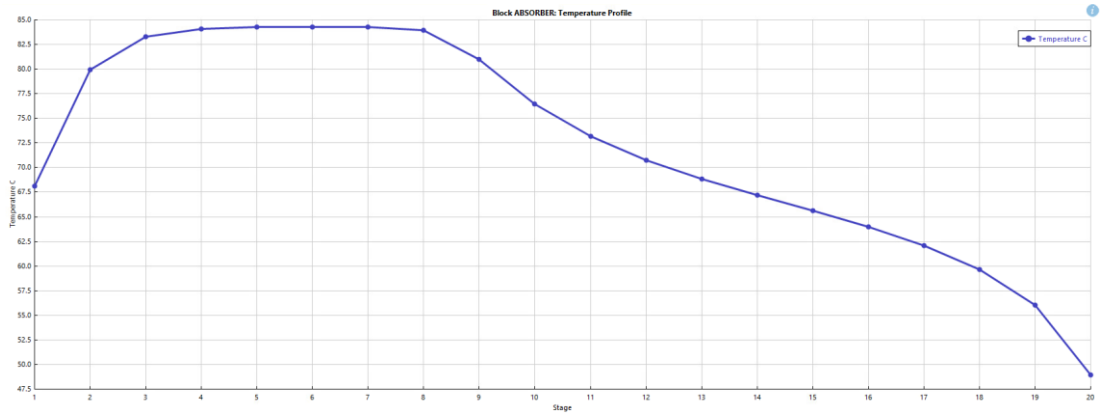

Figure 41. The temperature profile of the absorber in the 1 bar MEA once-through model.

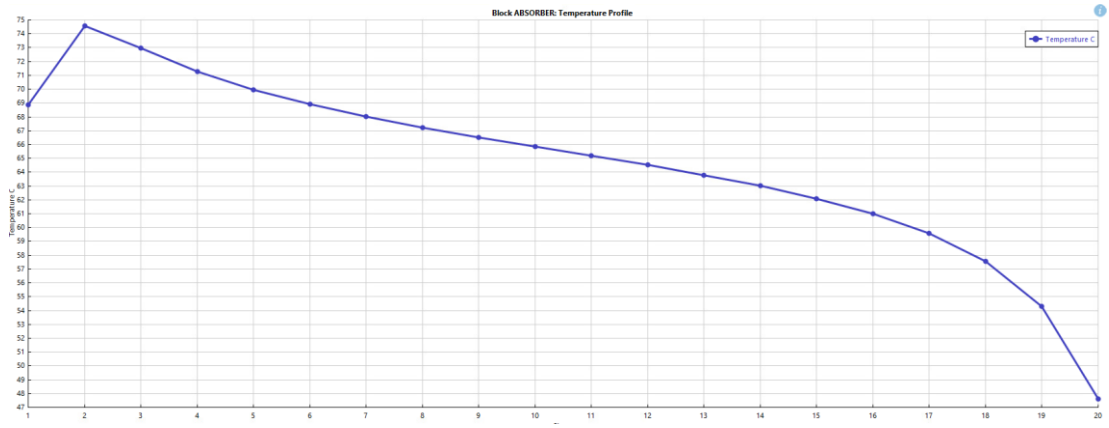

Figure 42. The temperature profile of the absorber in the finalized MEA model with recycling.

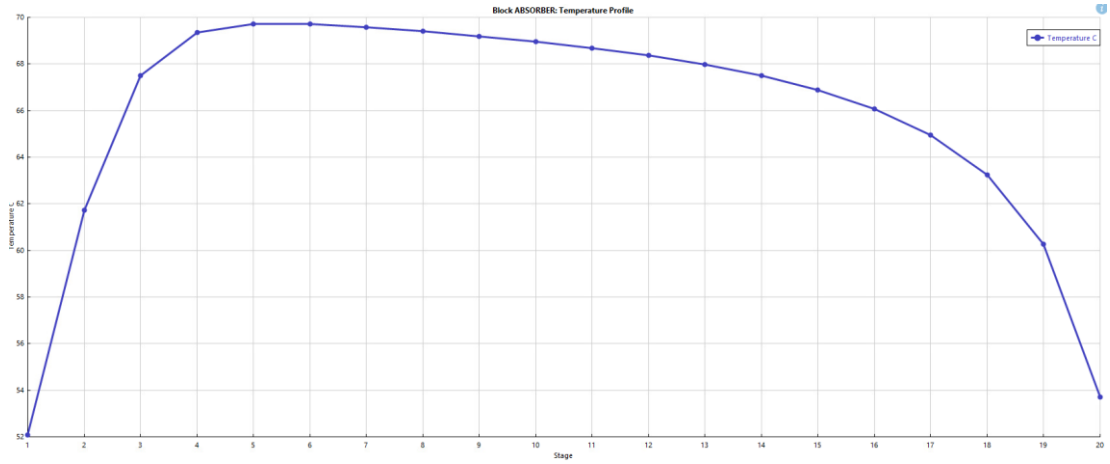

Figure 43. The temperature profile of the absorber in the finalized 1 bar MDEA once-through model.

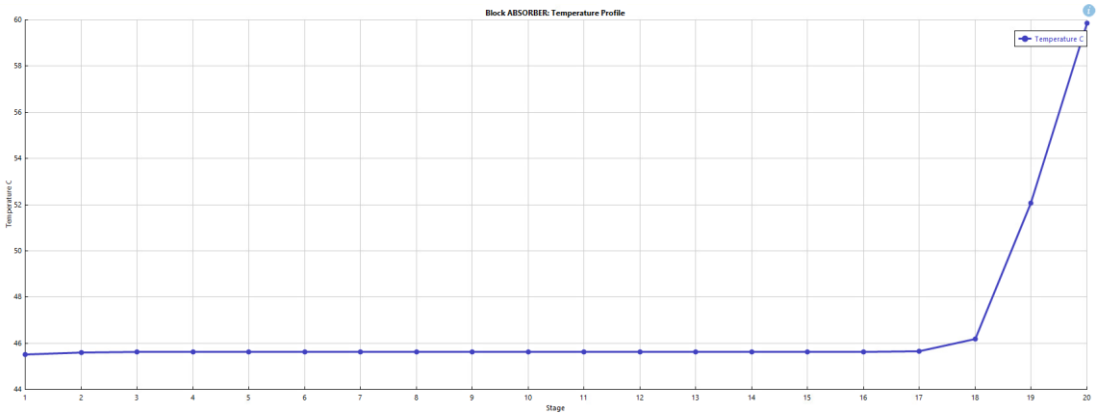

Figure 44. The temperature profile of the absorber in the finalized 15 bar MDEA once-through model.

The splitting of the relevant components within the absorber are shown in Tables 11-14.

Table 11. The splitting of substances within the absorber in the once-through MEA model.

		LHCHEAT	MEAFEED	LIGHTGAS	RICHAM
Mole Flows	kmol/hr	686.000	5800.000	750.758	5597.938
H2O	kmol/hr	0.193	5513.067	205.766	5274.093
H2	kmol/hr	288.333	0.000	288.219	0.114
CO2	kmol/hr	138.681	0.000	0.000	1.378
CO	kmol/hr	148.069	0.000	148.010	0.059
METHANE	kmol/hr	18.111	0.000	18.102	0.010
ETHANE	kmol/hr	3.897	0.000	3.849	0.048
PROPANE	kmol/hr	5.197	0.000	5.137	0.059
BUTANE	kmol/hr	4.422	0.000	4.061	0.360
ETHYLENE	kmol/hr	49.768	0.000	49.282	0.485
BUTYLENE	kmol/hr	15.591	0.000	14.519	1.072
PROPYLEN	kmol/hr	13.690	0.000	13.633	0.057
MEA	kmol/hr	0.000	286.933	0.131	42.113
MEA+	kmol/hr	0.000	0.000	0.000	140.786
H3O+	kmol/hr	0.000	0.000	0.000	0.000
MEACOO-	kmol/hr	0.000	0.000	0.000	103.904
OH-	kmol/hr	0.000	0.000	0.000	0.001
HCO3-	kmol/hr	0.000	0.000	0.000	29.919
CO3--	kmol/hr	0.000	0.000	0.000	3.481

Table 12. The splitting of substances within the absorber in the finalized MEA model with recycling.

		LHCHEAT	MEA	LIGHTGAS	RICHAM
Mole Flows	kmol/hr	686.000	5517.482	763.169	5304.587
H2O	kmol/hr	0.193	5200.813	217.466	4951.291
H2	kmol/hr	288.333	0.000	288.209	0.123
CO2	kmol/hr	138.681	0.000	1.450	1.505
CO	kmol/hr	148.069	0.000	148.004	0.064
METHANE	kmol/hr	18.111	0.000	18.101	0.011
ETHANE	kmol/hr	3.897	0.000	3.835	0.062
PROPANE	kmol/hr	5.197	0.000	5,109	0.088
BUTANE	kmol/hr	4.422	0.000	3.949	0.473
ETHYLENE	kmol/hr	49.768	0.000	49.140	0.627
BUTYLENE	kmol/hr	15.591	0.000	14.184	1.407
PROPYLEN	kmol/hr	13.690	0.000	13.619	0.071
MEA	kmol/hr	0.000	290.158	0.054	47.775
MEA+	kmol/hr	0.000	13.374	0.000	152.458
H3O+	kmol/hr	0.000	0.000	0.000	0.000
MEACOO-	kmol/hr	0.000	12.571	0.000	115.816
OH-	kmol/hr	0.000	0.233	0.000	0.001
HCO3-	kmol/hr	0.000	0.096	0.000	28.988
CO3--	kmol/hr	0.000	0.237	0.000	3.826

Table 13. The splitting of substances within the absorber in the 1 bar once-through MDEA model.

		LHCHEAT	LIGHTGAS	MDEAFEED	RICHAM
Mole Flows	kmol/hr	686.000	625.433	5800.000	5723.311
H2O	kmol/hr	0.193	79.895	5363.393	5146.431
H2	kmol/hr	288.333	288.294	0.000	0.039
CO2	kmol/hr	138.681	1.012	0.000	0.412
CO	kmol/hr	148.069	146.444	0.000	1.624
METHANE	kmol/hr	18.111	18.108	0.000	0.003
ETHANE	kmol/hr	3.897	3.893	0.000	0.004
PROPANE	kmol/hr	5.197	5.152	0.000	0.045
BUTANE	kmol/hr	4.422	4.262	0.000	0.160
ETHYLENE	kmol/hr	49.768	49.538	0.000	0.230
BUTYLENE	kmol/hr	15.591	15.114	0.000	0.476
PROPYLEN	kmol/hr	13.690	13.668	0.000	0.022
MDEA	kmol/hr	0.000	0.004	436.607	291.590
MDEA+	kmol/hr	0.000	0.000	0.000	145.013
H3O+	kmol/hr	0.000	0.000	0.000	0.000
OH-	kmol/hr	0.000	0.000	0.000	0.003
HCO3-	kmol/hr	0.000	0.000	0.000	129.504
CO3--	kmol/hr	0.000	0.000	0.000	7.753

Table 14. The splitting of substances within the absorber in the 15 bar once-through MDEA model.

		LHC	LIGHTGAS	MDEAFEED	RICHAM
Mole Flows	kmol/hr	686.000	505.432	5800.000	5845.086
H2O	kmol/hr	0.193	3.481	5588.771	5450.000
H2	kmol/hr	288.333	287.372	0.000	0.961
CO2	kmol/hr	138.681	0.000	0.000	3.199
CO	kmol/hr	148.069	115.462	0.000	32.606
METHANE	kmol/hr	18.111	18.040	0.000	0.072
ETHANE	kmol/hr	3.897	3.845	0.000	0.052
PROPANE	kmol/hr	5.197	4.794	0.000	0.402
BUTANE	kmol/hr	4.422	2.653	0.000	1.769
ETHYLENE	kmol/hr	49.768	46.279	0.000	3.488
BUTYLENE	kmol/hr	15.591	10.098	0.000	5.492
PROPYLEN	kmol/hr	13.690	13.361	0.000	0.329
MDEA	kmol/hr	0.000	0.000	211.229	72.711
MDEA+	kmol/hr	0.000	0.000	0.000	138.517
H3O+	kmol/hr	0.000	0.000	0.000	0.000
OH-	kmol/hr	0.000	0.000	0.000	0.001
HCO3-	kmol/hr	0.000	0.000	0.000	132.448
CO3--	kmol/hr	0.000	0.000	0.000	3.034

When trying to simulate with ethane and ethylene as the Henry components, only the simple once-through MEA model seems to sometimes work, and it gives results near those of Table 11. Quite often Aspen crashes completely and displays: “An error has occurred”, when trying to simulate with ethane and ethylene as Henry components. Within the stripper, it is more interesting to look at the capture rate of CO_2 compared to the entering CO_2 (LHC) and the lean loading of amine rather than every substance individually. Lean loading of each model and the capture rates are compiled in Table 15 as well as the reboiler and condenser duties.

Table 15. The capture rates and lean loading of each process model along with reboiler and condenser duties.

Process	Capture rate, %	Lean loading, %	Reboiler duty, kW	Condenser duty, kW
MEA, once-through	75.2	23.4	18105.6	-14616.9
MEA, recycling	99.0	6.9	113699	-111909
MDEA, 1 bar	93.6	1.8	30610	-26363.8
MDEA, 15 bar	99.6	0.5	38424.7	-35818.7

Finally, the results of cryogenic distillation are presented in Table 16.

Table 16. The results of cryogenic distillation.

		DISTIN	C2-C4	GASES
Mole Flows	kmol/hr	545.95	85.00	460.95
H2O	kmol/hr	0.35	0.35	0.00
H2	kmol/hr	288.19	0.00	288.19
CO2	kmol/hr	1.45	0.00	1.45
CO	kmol/hr	147.99	0.00	147.99
METHANE	kmol/hr	18.10	0.00	18.10
ETHANE	kmol/hr	3.84	3.81	0.02
PROPANE	kmol/hr	5.11	5.11	0.00
BUTANE	kmol/hr	3.95	3.95	0.00
ETHYLENE	kmol/hr	49.14	43.93	5.20
BUTYLENE	kmol/hr	14.18	14.18	0.00
PROPYLEN	kmol/hr	13.62	13.61	0.00

7. Discussion

7.1 Comparison of MEA and MDEA

When observing the absorber results and the temperature profiles, MEA and MDEA seem to be quite similar apart from the separation efficiency, as MDEA achieved a nearly 20 % higher capture capacity when comparing the once-through models. This could be since MEA is more appropriate for flue gas applications, while MDEA can be used more widely. It also seems like MDEA is able to regenerate a lot better in an equilibrium model setting than MEA, as the latter has considerably higher lean loading. However, when looking at the results of the simulation of the 15 bar MDEA model, it seems that Aspen does not handle the rise in pressure well, as the temperature profile turns quite illogical even when converging, when comparing to literature, for example, Figure 3 in the study of Moioli et al (2012). This assumption is further supported by the fact that if the simulation gets reset while the pressure is high and then rerun, it will not converge. It requires a previous simulation with a lower pressure as initial values to converge. Figures 41 and 42 are decently resemblant of the literature comparison.

Furthermore, it seems like the reaction between MEA and CO_2 happens substantially faster compared to MDEA and CO_2, as the temperatures rise higher and quicker in terms of stages in the MEA model. This could be due to the equilibrium model allowing the MEA reaction to progress further in comparison to the MDEA reaction. The observation is supported by the fact that MDEA w-% in the solution can be much higher than that of MEA, and the MDEA system is not as sensitive to changes, whereas the MEA model turns out to not converge even after little changes. This was noticed when 30 w-% MEA solution was tried out, as the temperature rose way too high, and it could not converge. Even entering the kinetics was tried out to help with the convergence and altering the reaction rate, but with kinetics the simulation could not converge at all. This could be due to the missing of column packing or because of the unique composition of substances in the process.

The K_2CO_3 process was also taken a brief look at, but the model did not start to converge, as CO_2 did not start reacting with water and potassium carbonate at all.

The templates provided by Aspen Plus V12.1 were not particularly helpful either, so it was excluded from the scope of this work.

7.2 Comparison to literature

In comparison to literature, MDEA seems to follow literature lean loading quite well, as Huttenhuis et al (2009) mention that MDEA lean loading can be as low as 2%. However, according to Choi et al. (2019), the lean loading of MEA is not too well in line with literature, as typical lean loading is between 0.2-0.3 molCO2/molMEA. This applies to the non-recycling model, but then the CO_2 removal efficiency is far behind the 88%, which is also mentioned in the study. This work was done with an equilibrium model, it is quite possible that a rate-based modelling approach would produce somewhat different results. In the study of Choi et al. (2019), a lot of different L/G ratios were tried out as well, ranging from 3 to nearly 10. This is an approval to the decision of choosing a molar ratio of 8.5.

7.3 Convergence problems

As demonstrated in Figure 42, the problems with the MEA model were usually those where the temperature profiles and results would not make any sense, as the simulation would not converge. The slightest changes in values could break the whole simulation and this was quite odd, as the formation enthalpies and other necessary parameter values were checked multiple times, therefore it should not be a thermodynamical problem. This is supported by the fact that the MDEA model is built using the MEA model as a template and it is much more forgiving with value changes and convergence apart from when recycling was implemented.

With the MEA model numerous fixes were tried, such as finding the formation enthalpies for all the ions and checking their integrity. Then, the NRTL values for water-ethylene system were regressed, which was a substantial help for convergence as well as integrity of the simulation in terms of the solubility of hydrocarbons in water (PubChem, 2023). The importance of temperature estimates for stages was emphasized as well, as the absorber model had trouble converging without supplying some estimates. It helps the computer to iterate closer to the real solution, as it gets to operate closer to the actual solution instead of starting from somewhere far.

Even kinetics were tried out to help with convergence, as in theory this should give more control over the reactions and how rapid they are. However, due to convergence problems, MEA and MDEA models both go into error, and Aspen gives the message "OH^- and H^+ ions are freezing" in the process of absorption, where the temperature should never go below 45 C, as that is the feed temperature, and the reaction is exothermic.

This is also why the "pump around loop" for water on top of the absorber was tried out. Mostly the model did not converge, although in one simulation it did, but it was problematic, as a substantial amount of water (nearly 1500 kmol/hr) escaped with light gases towards cryogenic distillation, so the idea of adding the loop was abandoned.

Various techniques were also tried to get the recycling to work, it was tried forcefully to close the loop with make-up streams and make it converge without any success. Additionally, it was tried with a splitter, increasing the recycling stream little by little, but that caused large accruals in hydrocarbons after a certain split fraction was surpassed. Another trick that was tried was to copy the LEANAM outlet stream into the inlet so that it would keep iterating, but this also had the same outcome as surpassing a certain split fraction. Furthermore, an old simulation was shown to me, where some CO_2 is added into the MEA inlet stream and the forum post of prof. Penteado also suggested that a small amount of CO_2 is pre-emptively added to set the lean amine to a situation where it is easier to find a convergence point. This allowed for the MEA model to converge and find a satisfying solution. However, the MDEA model would not converge even with this trick.

7.4 Integrity of the results

There is a fair amount of integrity to the results, as there are similarities to other studies and literature, but one should still read the results critically, as the simulation seems to be sensitive towards changes and modifications. This could be due to the uniqueness of the composition and perhaps there could even be parameters missing that have not been spotted during the work. However, the CO_2 capture rate of 99% for MEA might not be realistic with such a small amount of MEA, or the operating

costs would be excessively high, as the increased regeneration rate would greatly increase the reboiler and condenser duties. Furthermore, it is worth noticing that due to the increased pressure in the MDEA system, butylene and ethylene are exiting with the rich amine in substantial amounts, as well as a large share of the carbon monoxide, therefore it should not be seen as the best option. Additionally, the temperature profile in Figure 44 by itself shows that it is not trustable.

8. Conclusions and suggestions for the future

The goal of the thesis is to find methods to separate light hydrocarbons formed in a Fischer-Tropsch synthesis reactor from other light gases, ultimately resulting in olefins, paraffins, and C5+ hydrocarbons. The light gases would be recycled back into the Fischer-Tropsch reactor. In the literature part some of the technologies found in open literature were compared. In the comparison novel technologies were compared to more mature ones and the aim was to find two of the best ones to be investigated further in the applied part.

As the most critical separation in this process is the CO_2 removal from the hydrocarbon stream, the most attention was given to this issue. At the moment the most promising processes seem to be amine or hot carbonate scrubbing, but deep eutectic solvents and membrane technologies are evolving and could offer great alternatives in the future, as they get commercialised. However, in the light of the applied part of this work, it is fairly safe to say that MDEA outperforms MEA with this composition, as it shows greater capture efficiency, even though the recycling worked only for MEA.

The model could be further improved by making it a rate-based model and adding column packing along with the kinetics, as the kinetics and defining an adequate mass transfer model would help in sizing of the equipment. Perhaps the new modelling parameters such as hold-up on packing segments or mass transfer area could be used as parameters to be tuned for more stable simulations. Despite all the numerical problems encountered, the results obtained in the end are somewhat comparable to literature apart from the capture rate of once-through MEA model, but this could just be a flaw in the simulation, as it is a complex entity.

Bibliography

Adams II, T., Khojasteh, Y. 2015. Co-Production of Olefins, Fuels, and Electricity from Conventional Pipeline Gas and Shale Gas with Near-Zero CO2 Emissions. Part I: Process Development and Technical Performance. Energies. Vol. 8. Pp. 3739-3761. Available from: https://doi.org/10.3390/en8053739.

Ahn, H., Luberti, M., Liu, Z., Brandani, S. 2013. Process configuration studies of the amine capture process for coal-fired power plants. International Journal of Greenhouse Gas Control. Vol. 16. Pp. 29-40. Available from: https://doi.org/10.1016/j.ijggc.2013.03.002.

Akram, M., Milkowski, K., Gibbins, J., Pourkashanian, M. 2020. Comparative energy and environmental performance of 40 % and 30 % monoethanolamine at PACT pilot plant. International Journal of Greenhouse Gas Control. Vol. 95. Pp. 1-8. Available from: https://doi.org/10.1016/j.ijggc.2019.102946.

Alnashef, I., Abu-Zahra, M. R. M., Adeymi, I. 2017. Experimental Study of the Solubility of CO2 in Novel Amine Based Deep Eutectic Solvents. Energy Procedia. Vol. 105, pp. 1394-1400. Available from: https://doi.org/10.1016/j.egypro.2017.03.519.

Amghizar, A., Brown, D. J., Dedeyne, J. N., Marin, G. B., Van Geem, K. M. 2020. Sustainable innovations in steam cracking: CO_2 neutral olefin production. Reaction Chemistry & Engineering. Vol. 5:2. pp. 239-257. Available from: https://doi.org/10.1039/C9RE00398C.

Anthony, R. G.; McKetta, J. J. J. Chem. Eng. Data, 1967, 12, 17-20 Phase equilibria in the ethylene-water system. (Copy-pasted from Aspen Plus V12.1)

Baker, R. W., Lokhandwala, K. 2008. Natural Gas Processing with Membranes: An Overview. Industrial & Engineering Chemistry Research. Vol. 47:7, pp. 2109-2121. Available from: https://doi.org/10.1021/ie071083w.

Bastos-Neto, M., Siqueira, R. M., Freitas, G. R., Peixoto, H. R., do Nasicmento J. F., Musse, A. P. S., Torres, A. E. B., Azevedo, D. C. S. 2017. Carbon Dioxide Capture by Pressure Swing Adsorption. Energy Procedia. Vol. 114. pp. 2182-2192. Available from: https://doi.org/10.1016/j.egypro.2017.03.1355.

Bioplastics Magazine. 2020. The global bio-based polymer market in 2019 – A revised view [online]. [Referenced 14.3.2023]. Available from: https://www.bioplasticsmagazine.com/en/news/meldungen/20200127-The-global-bio-based-polymer-market-in-2019-A-revised-view.php.

Bradbury, E. J.; McNulty, D.; Savage, R. L.; McSweeney, E. E. Ind. Eng. Chem., 1952, 44, 211 The solubility of ethylene in water effect of temperature and pressure. (Copy-pasted from Aspen Plus V12.1)

Burr, B., Lyddon, L. 2008. A comparison of physical solvents for acid gas removal. Bryan Research and Engineering, Inc. Pp. 100-113. ISBN: 978-160560489-3.

Chakraborty, A., Kayal S. 2018. Activated carbon (type Maxsorb-III) and MIL-101(Cr) metal organic framework based composite adsorbent for higher CH_4 storage and CO_2 capture. Chemical Engineering Journal. Vol. 334. Pp. 780-788. Available from: https://doi.org/10.1016/j.cej.2017.10.080.

Chen, C. C., Que, H., Zhang, Y. 2011. Thermodynamic modeling for CO2 absorption in aqueous MEA solution with electrolyte NRTL model. Fluid Phase Equilibria. Vol. 311. Pp. 67-75. Available from: https://doi.org/10.1016/j.fluid.2011.08.025.

Choi, J. W., Trivedi, T. J., Lee, J. H., Lee, H. Y., Jeong, Y. K. 2016. Deep eutectic solvents as attractive media for CO2 capture. Green Chemistry. Vol. 18. Pp. 2834-2842. Available from: https://doi.org/10.1039/c5gc02319j.

Choi, J., Cho, H., Yun, S., Jang, M. G., Oh, S. Y., Binns, M., Kim J. K. 2019. Process design and optimization of MEA-based CO2 capture processes for non-power industries. Energy. Vol. 15. Pp. 971-980. Available from: https://doi.org/10.1016/j.energy.2019.07.092.

Davis, J. E.; McKetta, J. J. J. Chem. Eng. Data, 1960, 5, 374-375 Solubility of Ethylene in Water. (Copy-pasted from Aspen Plus V12.1)

Engineering ToolBox (ETB). 2018. Carbon Dioxide - Thermophysical Properties [online]. [Referenced 19.3.2023]. Available at: https://www.engineeringtoolbox.com/CO2-carbon-dioxide-properties-d_2017.html.

Feyzi, M., Khodaei, M. M., Shahmoradi, J. 2014. Effect of sulfur on the catalytic performance of Fe–Ni/Al_2O_3 catalysts for light olefins production. Journal of the Taiwan Institute of Chemical Engineers. Vol. 45:2. Pp. 452-460. Available from: https://doi.org/10.1016/j.jtice.2013.05.017.

ForestCUMP. 2022. Forest Industry Carbon dioxide Utilization for Materials and Plastics [online]. [Referenced 4.9.2023]. Available from: https://www.forestcu2mp.fi/about/.

Grande, C. A., Roussanaly, S., Anantharaman, R., Lindqvist, K., Singh, P., Kemper, J. CO_2 Capture in Natural Gas Production by Adsorption Processes. Energy Procedia. Vol. 114. pp. 2259-2264. Available from: https://doi.org/10.1016/j.egypro.2017.03.1363.

Hikita, H., Asai, S., Ishikawa, H., Honda, M. 1977. The Kinetics of Reactions of Carbon Dioxide with Monoethanolamine, Diethanolamine, and Triethanolamine by a Rapid Mixing Method. Chem. Eng. J. Vol. 13. Pp. 7-12. (From Aspen Plus V12.1 ENRTL-RK_RATE_BASED_MEA_MODEL.pdf)

Hilliard, M. A. 2008. A Predictive Thermodynamic Model for an Aqueous Blend of Potassium Carbonate, Piperazine, and Monoethanolamine for Carbon Dioxide. PhD Thesis, the University of Texas at Austin. (From Aspen Plus V12.1 ENRTL-RK_RATE_BASED_MEA_MODEL.pdf)

Hong, W. Y. 2022. A techno-economic review on carbon capture, utilisation and storage systems for achieving a net-zero CO_2 emissions future. Carbon Capture

Science & Technology. Vol 3. Pp. 1-28. Available from: https://doi.org/10.1016/j.ccst.2022.100044.

Hoorfar, M., Alcheikhhamdon, Y. 2017. Natural gas purification from acid gases using membranes: A review of the history, features, techno-commercial challenges, and process intensification of commercial membranes. Chemical Engineering and Processing – Process intensification. Vol. 120, pp. 105-113. Available from: https://doi.org/10.1016/j.cep.2017.07.009.

Huttenhuis, P. J. G., van Elk, E. P., Versteeg, P. G. 2009. Mass transfer in a small scale post-combustion flue gas absorber, experiment and modelling. Energy Procedia. Vol 1:1. Pp. 1131-1138. Available from: https://doi.org/10.1016/j.egypro.2009.01.149.

Jahanbakhsh-Bonab, P., Sardroodi, J. J., Avestan, M. S. 2022. The pressure effects on the Amine-Based DES performance in NG Sweetening: Insights from molecular dynamics simulation. Fuel. Vol. 323, pp. 1-12. Available from: https://doi.org/10.1016/j.fuel.2022.124249.

Kearns, D., Liu, H., Consoli, C. 2021. Technology Readiness and Costs of CCS [online]. Global CCS Institute. Pp. 4-48. [Referenced 13.4.2023]. Available from: https://www.globalccsinstitute.com/wp-content/uploads/2021/03/Technology-Readiness-and-Costs-for-CCS-2021-1.pdf.

Kim, J., Do, T. N. 2020. Green C_2-C_4 hydrocarbon production through direct CO_2 hydrogenation with renewable hydrogen: Process development and techno-economic analysis. Energy Conversion and Management. Vol. 214, pp. 1-11. Available from: https://doi.org/10.1016/j.enconman.2020.112866.

Kohl, A. L., Nielsen, R. B. 1997. Gas Purification. Gulf Publishing Company. Pp. 330-414. ISBN 9780080507200. Available from: https://discovery.ebsco.com/linkprocessor/plink?id=6adac2c8-6720-33c2-9b25-61c1208d2716.

Koros, W. J., Kim, T. H., Husk, G. R., O'Brien, K. C. 1988. Relationship between gas separation properties and chemical structure in a series of aromatic polyimides. Journal of Membrane Science. Vol. 37:1, pp. 45-62. Available from: https://doi.org/10.1016/S0376-7388(00)85068-1.

Lee, J. Y., Kim, S., Shi, H. 2016. CO_2 absorption mechanism in amine solvents and enhancement of CO_2 capture capability in blended amine solvent. International Journal of Greenhouse Gas Control. Vol. 45. Pp. 181-188. Available from: https://doi.org/10.1016/j.ijggc.2015.12.024.

Li, G., Xiao, J., Miao, G., Ma, Y., Yang, C., Tong, B. 2023. The effective synthesis of heat-pump assisted distillation process with multiple columns for light hydrocarbon separation. Chemical Engineering Science. Vol. 369. Pp. x-xx. Available from: https://doi.org/10.1016/j.ces.2023.118449.

Linde Engineering a. n.d. Adsorption, Membrane and Hybrid CC Technologies [online]. [Referred 22.3.2023]. Available from. https://www.linde-

engineering.com/en/process-plants/adsorption-and-membrane-plants/adsorption-based-carbon-capture-and-co2-recovery/index.html.

Linde Engineering b. n.d. HISELECT® powered by Evonik for ultra-efficient gas processing [online]. [Referred 22.3.2023]. Available from: https://www.linde-engineering.com/en/images/HISELECT-Evonik_tcm19-592594.pdf.

Linde Engineering c. n.d. HISORP® TS [online]. [Referred 22.3.2023]. Available from: https://www.linde-engineering.com/en/images/LE_AD_LINDE_HISORP_brochure_RZ_VIEW_44058_tcm19-592597.pdf.

Majone, M., Aulenta, F., Dionisi, D., D'Addario, E. N., Sbardellati, R., Bolzonella, D., Beccari, M. 2010. High-rate anaerobic treatment of Fischer-Tropsch wastewater in a packed-bed biofilm reactor. Water Research. Vol. 44:9. Pp. 2745-2752. Available from: https://doi.org/10.1016/j.watres.2010.02.008.

Maitlis, P. M., de Klerk, A. 2013. Greener Fischer-Tropsch Processes for Fuel and Feedstocks. Wiley-VCH. Pp. 19-392. ISBN 978-3-527-65686-8.

May, E. F., Rufford, T. E., Smart, S., Watson, G. C. Y., Graham, B. F., Boxall, J., Diniz da Costa, J.C. 2012. The removal of CO_2 and N_2 from natural gas: A review of conventional and emerging process technologies. Journal of Petroleum Science and Engineering. Vol. 94-95, pp. 123-154. Available from: https:doi.org/10.1016/j.petrol.2012.06.016.

Mcauliffe, C. J. Phys. Chem., 1966, 70, 1267-1275 Solubility in Water of Paraffin, Cycloparaffin, Olefin, Acetylene, Cycloolefin, and Aromatic Hydrocarbons. (Copy-pasted from Aspen Plus V12.1)

Mittal, V., George, G., Bhoria, N., AlHallaq, S., Abdala, A. 2015. Polymer membranes for acid gas removal from natural gas. Separation and Purification technology. Vol. 158, pp. 333-356. Available from: https://doi.org/10.1016/j.seppur.2015.12.033.

Moioli, S., Pellegrini, L. A., Gamba, S. 2012. Simulation of CO_2 Capture by MEA Scrubbing with a Rate-Based Model. Procedia Engineering. Vol 42. Pp. 1651-1661. Available from: https://doi.org/10.1016/j.proeng.2012.07.558.

Nakagaki, T., Isogai, H., Sato, H., Arakawa, J. 2019. Updated e-NRTL model for high-concentration MEA aqueous solution by regressing thermodynamic experimental data at high temperatures. International Journal of Greenhouse Gas Control. Vol. 82. Pp. 117-126. Available from: https://doi.org/10.1016/j.ijggc.2018.12.022.

Ochi, K.; Tada, M.; Kojima, K. Fluid Phase Equilib., 1990, 56, 341-359 Measurement and Correlation of Liquid-Liquid Equilibria Up to Critical Solution Temperature. (Copy-pasted from Aspen)

Official Statistics of Finland (OSF). 2021. Greenhouse Gases [online]. [Referenced 14.3.2023]. Available from: https://www.stat.fi/til/khki/2020/khki_2020_2021-12-16_kat_001_fi.html.

Oil & Gas Process Engineering. 2018. Benfield Process by UOP LLC [online]. [Referenced 27.8.2023]. Available from: http://www.oilngasprocess.com/gas/benfield-process-by-uop-llc.html.

Othmer, D. F.; White, R. E.; Trueger, E. Ind. Eng. Chem., 1941, 33, 1240-8 Liquid-liquid extraction data. (Copy-pasted from Aspen)

Paul, D. R., Chung, T.-S. Wang, H. 2014. Physical aging and plasticization of thick and thin films of the thermally rearranged ortho-functional polyimide 6FDA-HAB. Journal of Membrane Science. Vol. 458, pp. 27-35. Available from: https://doi.org/10.1016/j.memsci.2014.01.066.

Pinsent, B. R., Pearson, L., Roughton, F. J. W. 1956. The Kinetics of Combination of Carbon Dioxide with Hydroxide Ions. Trans. Faraday Soc. Vol. 52. Pp. 1512-1520. (From Aspen Plus V12.1 ENRTL-RK_RATE_BASED_MEA_MODEL.pdf)

Pubchem. 2023. Acetic acid [online]. [Referenced 19.3.2023]. Available from: https://pubchem.ncbi.nlm.nih.gov/compound/Acetic-acid.

PubChem. 2023. Butane [online]. [Referenced 19.3.2023]. Available from: https://pubchem.ncbi.nlm.nih.gov/compound/Butane.

PubChem. 2023. Butanoic Acid [online]. [Referenced 13.4.2023]. Available from: https://pubchem.ncbi.nlm.nih.gov/compound/Butyric-acid.

Pubchem. 2023. Butanol [online]. [Referenced 19.3.2023]. Available from: https://pubchem.ncbi.nlm.nih.gov/compound/1-butanol.

PubChem. 2023. Butene [online]. [Referenced 19.3.2023]. Available from: https://pubchem.ncbi.nlm.nih.gov/compound/1-Butene.

PubChem. 2023. Carbon dioxide [online]. [Referenced 19.3.2023]. Available from: https://pubchem.ncbi.nlm.nih.gov/compound/Carbon-dioxide.

PubChem. 2023. Carbon monoxide [online]. [Referenced 19.3.2023]. Available from: https://pubchem.ncbi.nlm.nih.gov/compound/Carbon-monoxide.

PubChem. 2023. Ethane [online]. [Referenced 19.3.2023]. Available from: https://pubchem.ncbi.nlm.nih.gov/compound/Ethane.

Pubchem. 2023. Ethanol [online]. [Referenced 19.3.2023]. Available from: https://pubchem.ncbi.nlm.nih.gov/compound/ethanol.

PubChem. 2023. Ethene [online]. [Referenced 19.3.2023]. Available from: https://pubchem.ncbi.nlm.nih.gov/compound/Ethylene.

PubChem. 2023. Heptene [online]. [Referenced 19.3.2023]. Available from: https://pubchem.ncbi.nlm.nih.gov/compound/1-Heptene.

PubChem. 2023. Hexane [online]. [Referenced 19.3.2023]. Available from: https://pubchem.ncbi.nlm.nih.gov/compound/n-HEXANE.

PubChem. 2023. Hexene [online]. [Referenced 19.3.2023]. Available from: https://pubchem.ncbi.nlm.nih.gov/compound/1-Hexene.

PubChem. 2023. Hydrogen [online]. [Referenced 19.3.2023]. Available from: https://pubchem.ncbi.nlm.nih.gov/compound/Hydrogen.

PubChem. 2023. Methane [online]. [Referenced 19.3.2023]. Available from: https://pubchem.ncbi.nlm.nih.gov/compound/Methane.

Pubchem. 2023. Methanol [online]. [Referenced 19.3.2023]. Available from: https://pubchem.ncbi.nlm.nih.gov/compound/methanol.

PubChem. 2023. Octene [online]. [Referenced 19.3.2023]. Available from: https://pubchem.ncbi.nlm.nih.gov/compound/1-Octene.

PubChem. 2023. Pentane [online]. [Referenced 19.3.2023]. Available from: https://pubchem.ncbi.nlm.nih.gov/compound/Pentane.

Pubchem. 2023. Pentanol [online]. [Referenced 19.3.2023]. Available from: https://pubchem.ncbi.nlm.nih.gov/compound/1-Pentanol.

PubChem. 2023. Pentene [online]. [Referenced 19.3.2023]. Available from: https://pubchem.ncbi.nlm.nih.gov/compound/1-Pentene.

PubChem. 2023. Propane [online]. [Referenced 19.3.2023]. Available from: https://pubchem.ncbi.nlm.nih.gov/compound/Propane.

Pubchem. 2023. Propanol [online]. [Referenced 19.3.2023]. Available from: https://pubchem.ncbi.nlm.nih.gov/compound/1-propanol.

PubChem. 2023. Propene [online]. [Referenced 19.3.2023]. Available from: https://pubchem.ncbi.nlm.nih.gov/compound/Propylene.

Pubchem. 2023. Propionic Acid [online]. [Referenced 13.4.2023]. Available from: https://pubchem.ncbi.nlm.nih.gov/compound/Propionic-Acid.

Researchgate. 2015. How can I overcome a simulation problem with Aspen Plus? [online]. [Referenced 27.8.2023]. Available from: https://www.researchgate.net/post/How_can_I_overcome_a_simulation_problem_with_Aspen_Plus.

Rezakazemi, M., Heydari, I., Zhang, Z. 2017. Hybrid systems: Combining membrane and absorption technologies leads to more efficient acid gases (CO2 and H2S) removal from natural gas. Journal of CO2 Utilization. Vol. 18, Pp. 362-369. Available from: https://doi.org/10.1016/j.jcou.2017.02.006.

Riboldi, L., Bolland, O. 2017. Overview on Pressure Swing Adsorption (PSA) as CO_2 Capture Technology: State-of-the-Art, Limits and Potentials. Energy Procedia. Vol. 114. Pp. 2390-2400. Available from: https://doi.org/10.1016/j.egypro.2017.03.1385.

Robeson, L. M. 1991. Correlation of separation factor versus permeability for polymeric membranes. Journal of Membrane Science. Vol. 62:2, pp. 165-185. Available from: https://doi.org/10.1016/0376-7388(91)80060-J.

Rommens, K. T., Saeys, M. 2023. Molecular Views on Fischer-Tropsch Synthesis. Chemical Reviews. Vol. x:x. pp. A-AV. Available from: https://doi.org/10.1021/acs.chemrev.2c00508.

Sanchez, M.; Lentz, H. High Temp. - High Pressures, 1973, 5, 689-99 Phase equilibrium of water + propane and water + ethane systems at high temperatures and pressures. (Copy-pasted from Aspen Plus V12.1)

Scholes, C. A., Lee, Y. M., Dong, G., Kim, J. S., Jo, H. J., Lee, J. 2017. Permeation and separation of SO2, H2S and CO2 through thermally rearranged (TR) polymeric membranes. Separation and Purification Technology. Vol. 179, pp. 449-454. Available from. https://doi.org/10.1016/j.seppur.2016.12.039.

Shahid, M. Z., Maulud, A. S., Bustam, M. A., Suleman, H., Halim, H. Z. A., Shariff, A. M. 2019. Rate-Based Modeling for Packed Absorption Column of the MEA-CO_2-Water System at High-Pressure and High-CO_2 Loading Conditions. Industrial and Engineering Chemistry Research. Vol. 58:27. Pp. 12235-12246. Available from: https://doi.org/10.1021/acs.iecr.9b01482.

Skogestad, S., Solvik, M., Reyes-Lúa A. 2016. Inclusion of thermodynamic equations for efficient steadystate process optimization. Computer Aided Chemical Engineering. Vol. 38. Pp. 613-618. Available from: https://doi.org/10.1016/B978-0-444-63428-3.50107-7.

Smith, K. H., Nicholas, N. J., Stevens, G. W. 2016. Absorption-Based Post-combustion Capture of Carbon Dioxide. Woodhead Publishing. Pp. 145-166. ISBN 9780081005149. Available from: https://doi.org/10.1016/B978-0-08-100514-9.00007-X.

Smithson, C. 2023. Natural Gas Composition [online]. [Referenced 21.4.2023]. Available from: https://www.croftsystems.net/oil-gas-blog/natural-gas-composition/.

Sohrabi, M., Tavakoli, A., Kargari, A. 2008. Application of Anderson–Schulz–Flory (ASF) equation in the product distribution of slurry phase FT synthesis with nanosized iron catalysts. Chemical Engineering Journal. Vol 136:2-3. pp. 358-363. Available from: https://doi.org/10.1016/j.cej.2007.04.017.

Song, C., Pan, W., Srimat, S. T., Zheng, J., Li, Y., Wang, Y. H., Xu, B. Q., Zhu, Q. M. 2004. Tri-reforming of methane over Ni Catalysts for CO_2 Conversion to Syngas With Desired H_2/CO Ratios Using Flue Gas of Power Plants Without CO_2 Separation. Studies in Surface Science and Catalysis. Vol. 153. Pp. 315-322. Available from: https://doi.org/10.1016/S0167-2991(04)80270-2.

Speight, J.G. 2007. Natural gas. Gulf Publishing Company. Pp. 161-192. ISBN 9781933762142. Available from: https://doi.org/10.1016/B978-1-933762-14-2.50012-1.

Speight, J. G. 2019. Natural Gas (Second edition). Gulf Professional Publishing. Pp. 277-324. ISBN 9780128095706. Available from: https://doi.org/10.1016/B978-0-12-809570-6.00008-4.

Statista. 2022. Market volume of polyethylene worldwide from 2015 to 2021, with a forecast for 2022 to 2029 [online]. [Referenced 14.3.2023]. Available from: www.statista.com/statistics/1245162/polyethylene-market-volume-worldwide/.

Statista. 2022. Market volume of polypropylene worldwide from 2015 to 2021, with a forecast for 2022 to 2029 [online]. [Referenced 14.3.2023]. Available from: www.statista.com/statistics/1245169/polypropylene-market-volume-worldwide/.

Telfer, S. G., Babarao, R., Qazvini, O. T. 2021. Selective capture of carbon dioxide from hydrocarbons using a metal-organic framework. Nature Communications. Vol. 12:197. Pp. 1-8. Available from: https://doi.org/10.1038/s41467-020-20489-2.

The Engineering ToolBox. 2008. Ethane – Thermophysical Properties. [online] Available at: https://www.engineeringtoolbox.com/ethane-d_1417.html. [Accessed 27.8.2023]

The Engineering ToolBox. 2018. Ethylene – Thermophysical Properties. [online] Available at: https://www.engineeringtoolbox.com/ethylene-ethene-C2H4-properties-d_2104.html. [Accessed 27.8.2023]

Tcvetkov, P. 2021. Climate Policy Imbalance in the Energy Sector: Time to Focus on the Value of CO_2 Utilization. Energies. Vol. 14:2. Pp. 1-22. Available from: https://doi.org/10.3390/en14020411.

Tsiklis, D. S.; Kulikova, A. I.; Shenderei, L. I. Khim. Prom-st. (Moscow), 1960, , 401-6 Phase equilibria in the system ethanol + ethylene + water at high pressures and temperatures. (Copy-pasted from Aspen Plus V12.1)

UOP Honeywell. n.d. Gas Processing [online]. [Referenced 21.4.2023]. Available from: https://uop.honeywell.com/en/equipment-and-aftermarket-services/aftermarket/gas-processing/spare-parts-consumables-and-services.

Wang, Y., Sun, W., Webb, E., Xu, G., Zhang, W., Zhao, X. 2023. Advances in metal-organic framework-based hydrogel materials: preparation, properties and applications. Journal of Materials Chemistry A. Vol. 11:5. Pp. 2092-2127. Available from: https://doi.org/10.1039/D2TA08841J.

Wu, Y., Xie, L. H., Liu, X. M. 2023. Efficient Propylene/Ethylene Separation in Highly Porous Metal-Organic Frameworks. Materials. Vol 16:1. Pp. 1-13. Available from: https://doi.org/10.3390/ma16010154.

Zongbi, B., Fuqiang, C., Kaiqing, G., Xinlei, H., Zhiguo, Z., Qiwei, Y., Yiwen, Y., Qilong, R. 2023. Extraction of propane and ethane from natural gas on ultramicroporous carbon adsorbent with record selectivity. Science China Materials. Vol. 66:1. Pp. 319-326. Available from: https://doi.org/10.1007/s40843-022-2096-8.